Inorg. Chem. **2008**, *47*, 3903−3919

Tetra-2,3-pyrazinoporphyrazines with Externally Appended Pyridine Rings. 5. Synthesis, Physicochemical and Theoretical Studies of a Novel Pentanuclear Palladium(II) Complex and Related Mononuclear Species

Maria Pia Donzello,[†] Elisa Viola,[†] Xiaohui Cai,[‡] Luisa Mannina,[§,II] Corrado Rizzoli,[⊥] Giampaolo Ricciardi,[#] Claudio Ercolani,*[,†] Karl M. Kadish,*[,‡] and Angela Rosa*[,#]

Dipartimento di Chimica, Università degli Studi di Roma "La Sapienza", Piazzale A. Moro 5, I-00185 Roma, Italy, Department of Chemistry, University of Houston, Houston, Texas 77204-5003, Dipartimento di STAAM, Università degli Studi del Molise, via De Sanctis, I-8610 Campobasso, Italy, Istituto di Metodologie Chimiche, CNR, I-00016 Monterotondo Staz., Roma, Italy, Dipartimento di Chimica Generale ed Inorganica, Università di Parma, viale G. P. Usberti 17-A, I-43100 Parma, Italy, and Dipartimento di Chimica, Università della Basilicata, Via N. Sauro 85, I-85100 Potenza, Italy

Received December 17, 2007

New palladium(II) complexes of the free-base tetrakis[2,3-(5,6-di-2-pyridylpyrazino)porphyrazine], [$Py_8TPyzPzH_2$], have been prepared and their physicochemical properties examined. The investigated compounds are the pentanuclear species [$(PdCl_2)_4Py_8TPyzPzPd$], the monopalladated complex [$Py_8TPyzPzPd$], and its corresponding octaiodide salt [(2-Mepy)$_8$TPyzPzPd](I)$_8$. All three Pd^{II} complexes have a common central pyrazinoporphyrazine core and differ only at the periphery of the macrocycle, where the simple dipyridinopyrazine fragments present in [$Py_8TPyzPzPd$] bear four $PdCl_2$ units coordinated at the pyridine N atoms in the pentanuclear complex, [$(PdCl_2)_4Py_8TPyzPzPd$], or carry pyridine−$N(CH_3)^+$ moieties in the iodide of the octacation [(2-Mepy)$_8$TPyzPzPd]$^{8+}$. The structural features of the pentanuclear complex [$(PdCl_2)_4Py_8TPyzPzPd$], partly supported by X-ray data and solution ^{1}H NMR spectra of the [$(CN)_2Py_2PyzPdCl_2$] precursor, were elucidated through one- and two-dimensional ^{1}H NMR spectra in solution and density functional theory (DFT) calculations. Structural information on the monopalladated complex [$Py_8TPyzPzPd$] was also obtained from DFT calculations. It was found that in the complex [$(PdCl_2)_4Py_8TPyzPzPd$] the peripheral $PdCl_2$ units adopt a py−py coordination mode and the generated N_2PdCl_2 moieties are directed nearly perpendicular to the plane of the pyrazinoporphyrazine ring, strictly recalling the arrangement found for the palladated precursor [$(CN)_2Py_2PyzPdCl_2$]. NMR and DFT results consistently indicate that of the four structural isomers predictable for [$(PdCl_2)_4Py_8TPyzPzPd$], one having all four N_2PdCl_2 moieties pointing on the same side of the macrocyclic framework (i.e., isomer 4:0, plus the 3:1 and the 2:2-cis and 2:2-trans isomers), the 4:0 isomer (C_{4v} symmetry) is the predominant form present. According to cyclic voltammetry and spectroelectrochemical results in pyridine, dimethyl sulfoxide (DMSO), and dimethylformamide (DMF), the monopalladated complex [$Py_8TPyzPzPd$] undergoes four reversible or quasi-reversible one-electron ligand-centered reductions, similar to the behavior also observed for the pentanuclear complex [$(PdCl_2)_4Py_8TPyzPzPd$], which shows an additional reduction peak attributable to the presence of $PdCl_2$. Owing to the electron-withdrawing properties of the $PdCl_2$ units, the pentanuclear complex is easier to reduce than the mononuclear complex [$Py_8TPyzPzPd$], some related [$Py_8TPyzPzM$] complexes, and their porphyrin or porphyrazine analogues, so much so that the corresponding monoanion radical is generated at potentials close to 0.0 V vs SCE in DMSO or DMF. In turn, the monoanion of [(2-Mepy)$_8$TPyzPzPd](I)$_8$ is also extremely easy to generate electrochemically. Indeed, because of the eight positively charged N-CH_3^+ groups in this complex the first reduction occurs at potentials close to +0.10 V in DMSO or DMF. The redox behavior of the mono- and pentapalladated complexes has been rationalized on the basis of a detailed DFT analysis of their ground-state electronic structure.

Introduction

Our recent studies have been directed toward the synthesis and characterization of a novel series of porphyrazine macrocycles carrying externally annulated five-, six-, and seven-membered electron-deficient heterocycles.[1] Among the examined compounds were the free-base tetrakis[2,3-(5,6-di-2-pyridylpyrazino)porphyrazine], [$Py_8TPyzPzH_2$],[1b] its metal derivatives [$Py_8TPyzPzM$] where M = $Mg^{II}(H_2O)$,

* To whom correspondence should be addressed. E-mail: claudio.ercolani@uniroma1.it.
† Università degli Studi di Roma "La Sapienza".
‡ University of Houston.
§ Università degli Studi del Molise.
II Istituto di Metodologie Chimiche, CNR.
⊥ Università di Parma.
Università della Basilicata.

10.1021/ic702430j CCC: $40.75
Published on Web 05/05/2008

Scheme 1. Schematic Representation of (A) the Neutral Complexes $[Py_8TPyzPzM]$[1b,c] and (B) Their Corresponding Octacations $[(2\text{-}Mepy)_8TPyzPzM]^{8+}$ (Salted by I^- Ions)[1d,e]

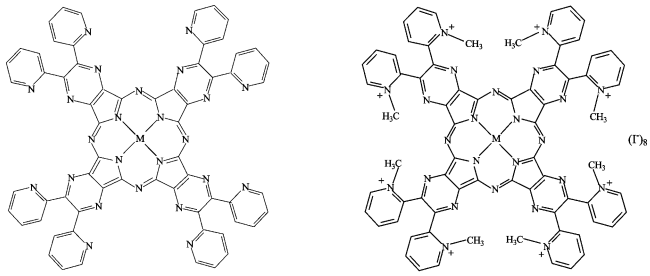

A B

Mn^{II}, Co^{II}, Cu^{II} or Zn^{II} (Scheme 1A),[1c] and the related octacationic species $[(2\text{-}Mepy)_8TPyzPzM]^{8+}$ (neutralized by I^- anions; Scheme 1B), where the N pyridine atoms are present in the methylated form $\equiv NCH_3^+$.[1d,e]

In a further extension of this work, the synthesis of metal derivatives in the d^8 triad, i.e., Ni^{II}, Pd^{II}, and Pt^{II}, was also planned. However, attempts to prepare the monometalated complexes $[Py_8TPyzPzNi]$ and $[Py_8TPyzPzPt]$ encountered difficulties with complete incorporation of the metal ions into the central cavity of the free-base macrocycle. This was not the case for Pd^{II}, and we here report the synthesis of the monopalladated complex $[Py_8TPyzPzPd]$, its octacation $[(2\text{-}Mepy)_8TPyzPzPd]^{8+}$ (neutralized by I^- anions), and a pentapalladated species having the formula $[(PdCl_2)_4Py_8TPyzPzPd]$. The three complexes, which were obtained in the sequence $[(PdCl_2)_4Py_8TPyzPzPd] \rightarrow [Py_8TPyzPzPd] \rightarrow [(2\text{-}Mepy)_8TPyzPzPd](I)_8$, were characterized by elemental and thermogravimetric analyses (TGA), IR, and UV–visible spectroscopy.

Insights into the molecular structure of the pentametallic species $[(PdCl_2)_4Py_8TPyzPzPd]$, a complex showing quite a rare example of exocyclic metal coordination, were gained through a combination of one- and two-dimensional ^1H NMR spectroscopy, density functional theory (DFT) calculations, and X-ray studies on the $[(CN)_2Py_2PyzPdCl_2]$ precursor. ^1H NMR structural analysis of the monopalladated complex was prevented by aggregation phenomena and/or insufficient solubility in organic solvents. Information on the molecular structure of this species was achieved by DFT calculations. The electrochemistry and spectroelectrochemistry of the three Pd^{II} complexes were investigated in pyridine, dimethyl sulfoxide (DMSO), and dimethylformamide (DMF). For $[(PdCl_2)_4Py_8TPyzPzPd]$ and $[Py_8TPyzPzPd]$, a detailed theoretical analysis of the ground-state electronic structure was also performed, which allowed for a rationalization of their redox behavior.

In view of a possible use of the title palladium(II) complexes in photodynamic therapy,[2] their singlet-oxygen photosensitizing properties have also been investigated. These studies are reported in a forthcoming paper.[3] It is anticipated here that all three complexes, particularly $[(PdCl_2)_4Py_8TPyzPzPd]$ and $[Py_8TPyzPzPd]$, show very high singlet-oxygen quantum yields.

Experimental Section

Solvents and Reagents. Solvents and chemicals were used as purchased, unless otherwise indicated. $[(C_6H_5CN)_2PdCl_2]$ was prepared as reported.[4] The precursor 2,3-dicyano-5,6-di-2-pyridyl-1,4-pyrazine, $[(CN)_2Py_2Pyz]$, and the free-base macrocycle $[Py_8TPyzPzH_2]\cdot 4H_2O$ were synthesized as previously described.[1b]

Synthesis of $[(CN)_2Py_2PyzPdCl_2]$. The precursor 2,3-dicyano-5,6-di-2-pyridyl-1,4-pyrazine, $[(CN)_2Py_2Pyz]$ (210 mg, 0.74 mmol), was dissolved in CH_3OH (15 mL) at room temperature. A suspension of $[(C_6H_5CN)_2PdCl_2]$ (310 mg, 1.08 mmol) in CH_3OH (15 mL) was added to solution and the formation of a precipitate was immediately observed. The solid was separated by centrifugation, washed with methanol, and brought to a constant weight under vacuum (10^{-2} mmHg) (295 mg, yield 86%). Calcd for $[(CN)_2Py_2PyzPdCl_2]$, $C_{16}H_8Cl_2N_6Pd$: C, 41.63; H, 1.75; N, 18.21; Pd, 23.05. Found: C, 41.88; H, 2.05; N, 18.39; Pd, 23.34. IR (KBr, cm^{-1}): ca. 3440 w (very broad), 3107 vw, 3049 w, 1622 m, 1598 m, 1569 w, 1524 w, 1486 m, 1439 w, 1383 vs, 1291 w, 1248 m, 1192 m, 1161 w, 1142 w, 1112 wm, 1097 m, 1057 w, 1033 w, 966 vw, 904 vw, 816 w, 780 s, 765 m, 756 m, 743 vw, 689 w, 662 w, 609 w, 572 w, 552 w, 530 w, 494 vw, 451 vw, 435 vw, 340, 335 m-s/split ν(Pd−Cl). MALDI-TOF $[M + H]^+$: *m*/*z* 285.26 ($M = 284.28$, molecular weight of the demetalated precursor; see the discussion below). The complex gave crystals suitable for X-ray work by recrystallization from hot CH_3CN.

Synthesis of $[(PdCl_2)_4Py_8TPyzPzPd]\cdot 10H_2O$. The free-base macrocycle $[Py_8TPyzPzH_2]\cdot 4H_2O$ (324 mg, 0.28 mmol) was suspended (partly dissolved) in DMSO which had been freshly distilled over CaH_2 (8 mL). After the addition of $PdCl_2$ (341 mg, 1.92 mmol), the mixture was heated at 120 °C for 5 h. After cooling, the solid material was separated by centrifugation, washed with water and acetone, and brought to a constant weight under vacuum (10^{-2} mmHg) (490 mg, yield 80%). Calcd for $[(PdCl_2)_4Py_8TPyzPzPd]\cdot 10H_2O$, $C_{64}H_{52}Cl_8N_{24}O_{10}Pd_5$: C, 36.04; H, 2.46; N, 15.76; Pd, 24.95. Found: C, 36.04; H, 2.60; N, 15.40; Pd, 24.35. TGA shows a 8.40% weight loss (water) in the range 25–100 °C (calcd for $10H_2O$: 8.44%). IR (KBr, cm^{-1}): 3400 w (very broad), 1604 w, 1557 m-s, 1516 m, 1483 w, 1358 vs, 1247 vs, 1189 s, 1167 w, 1130 s, 1057 vw, 1037 w, 969 m-s, 881 w, 814 w, 774 s, 752 m, 714 vs, 655 w, 559 m, 510 vw, 438 w, 349, 341 m-s/split ν(Pd−Cl).

It was observed that release of the peripheral $PdCl_2$ groups occurred upon dissolution of the pentapalladated species in pyridine

(1) (a) Donzello, M. P.; Ercolani, C.; Stuzhin, P. A. *Coord. Chem. Rev.* **2006**, *250*, 1530–1561, and references cited therein. (b) Donzello, M. P.; Ou, Z.; Monacelli, F.; Ricciardi, G.; Rizzoli, C.; Ercolani, C.; Kadish, K. M. *Inorg. Chem.* **2004**, *43*, 8626. (c) Donzello, M. P.; Ou, Z.; Dini, D.; Meneghetti, M.; Ercolani, C.; Kadish, K. M. *Inorg. Chem.* **2004**, *43*, 8637. (d) Bergami, C.; Donzello, M. P.; Ercolani, C.; Monacelli, F.; Kadish, K. M.; Rizzoli, C. *Inorg. Chem.* **2005**, *44*, 9852. (e) Bergami, C.; Donzello, M. P.; Monacelli, F.; Ercolani, C.; Kadish, K. M. *Inorg. Chem.* **2005**, *44*, 9862. (f) Donzello, M. P.; Ercolani, C.; Stuzhin, P. A.; Chiesi-Villa, A.; Rizzoli, C. *Eur. J. Inorg. Chem.,* **1999**, 2075. (g) Donzello, M. P.; Dini, D.; D'Arcangelo, G.; Zhan, R.; Ou, Z.; Ercolani, C.; Stuzhin, P. A.; Kadish, K. M. *J. Am. Chem. Soc.* **2003**, *125*, 14190. (h) Villano, M.; Amendola, V.; Sandonà, G.; Donzello, M. P.; Ercolani, C.; Meneghetti, M. *J. Phys. Chem. B* **2006**, *110*, 24534.

(2) (a) Szacilowski, K.; Macyk, W.; Drzewiecka-Matuszek, A.; Brindell, M.; Stochel, G. *Chem. Rev.* **2005**, *105*, 2647–2694. (b) Detty, M. R.; Gibson, S. L.; Wagner, S. J. *J. Med. Chem.* **2004**, *47*, 3897–3915. (c) De Rosa, M. C.; Crutchley, R. J. *Coord. Chem. Rev.* **2002**, *234*, 351–371.

(3) Donzello, M. P.; et al., manuscript in preparation.

(4) Kharasch, M. S.; Seyler, R. C.; Mayo, F. R. *J. Am. Chem. Soc.* **1938**, *60*, 882.

at room temperature. This was verified by stirring of the solution containing the compound up to complete evaporation of the solvent and by characterization of the products after final desiccation of the solid material under vacuum. The solid formed was found to consist of a mixture of the monopalladated complex [Py_8TPyzPzPd] (hydrated) and the pyridine complex [$(Py)_2PdCl_2$]. [$(Py)_2PdCl_2$] was separated from the macrocycle by washing with warm acetone (50 °C) and, after removal of the solvent, identified by elemental analyses, IR spectra, and comparison with an analogous material prepared separately by the simple addition of pyridine to $PdCl_2$. [Py_8TPyzPzPd] was easily identified by its IR spectrum and elemental analyses. A MALDI-TOF spectrum of the solid penta-palladated species showed no peaks with the molecular weight of the compound and only a peak for the monopalladated species was observed (M = 1243.54), indicating loss of the four $PdCl_2$ units during irradiation of the sample. Loss of $PdCl_2$ also occurred when measuring the MALDI-TOF spectrum of the palladated precursor [$(CN)_2Py_2PyzPdCl_2$]. In this case, only a peak for the demetalated precursor [$(CN)_2Py_2Pyz$] was detected in the spectrum.

Synthesis of [Py_8TPyzPzPd]·$6H_2O$ by Demetalation of Exocyclic $PdCl_2$ Groups from [$(PdCl_2)_4Py_8$TPyzPzPd]·$10H_2O$. [$(PdCl_2)_4Py_8$TPyzPzPd]·$10H_2O$ (112 mg, 0.053 mmol) was suspended in a 3% NH_3 aqueous solution (1.5 mL) and stirred for 2 h at room temperature. After centrifugation, the solid material was washed with water to neutrality and then with acetone and brought to a constant weight under vacuum (10^{-2} mmHg) (40 mg, yield 56%). Calcd for [Py_8TPyzPzPd]·$6H_2O$, $C_{64}H_{44}N_{24}O_6Pd$: C, 56.87; H, 3.28; N, 24.87; Pd, 7.87. Found: C, 56.65; H, 2.11; N, 25.01; Pd, 7.77. TGA shows a 7.40% weight loss (water) in the range 25–100 °C (calcd for $6H_2O$: 7.99%). IR (KBr, cm^{-1}): 3400 w (very broad), 1627 w, 1584 m, 1551 m, 1509 w, 1461 m, 1433 w-m, 1417 w, 1360 vs, 1296 vw, 1245 vs, 1194 m, 1126 vs, 1052 w, 993 m-s, 972 m-s, 876 w, 829 w, 790 vs, 744 s, 716 vs, 665 w, 630 vw, 605 vw, 560 m, 438 w, 405 vw. MALDI-TOF $[M + H]^+$: m/z 1244.55 (M = 1243.54).

Synthesis of [(2-Mepy)$_8$TPyzPzPd](I)$_8$(H_2O). [Py_8TPyzPzPd]·$6H_2O$ (20 mg, 0.0148 mmol) and CH_3I (0.20 mL, 3.2 mmol) were added to DMF (1 mL), and the mixture was kept at room temperature for 4 days. After evaporation of the excess CH_3I in air at room temperature, a precipitate was separated, washed with benzene, and brought to a constant weight under vacuum (10^{-2} mmHg) (27.4 mg, yield 76%). Calcd for [(2-Mepy)$_8$TPyzPzPd](I)$_8$(H_2O), $C_{72}H_{58}I_8N_{24}OPd$: C, 36.08; H, 2.44; N, 14.02; Pd, 4.44. Found: C, 36.58; H, 2.37; N, 14.59; Pd, 5.33. IR (KBr, cm^{-1}): 3440 w-m (broad), 3030 w, 3012 w, 1625 m, 1585 m, 1550 w, 1515 w-m, 1484 vw, 1458 w-m, 1436 w, 1359 s, 1250 vs, 1190 w-m, 1130 w, 1090 vw, 997 m, 970 m, 945 m, 880 vw, 826 vw, 787 m-s, 746 w, 720 m, 690 w, 660 w, 600 vvw, 569 w, 510 vw, 440 w.

X-ray Crystallography of [$(CN)_2Py_2PyzPdCl_2$]. Crystal data on the complex were collected on a Bruker SMART 1000 CCD diffractometer using graphite-monochromatized Mo Kα radiation at 293 K. The solution and refinement were carried out using the programs *SIR97*[5] and *SHELX97*.[6]

^{1}H NMR. ^{1}H NMR spectra were taken in DMF solutions (99.5% DMF-d_7 CIL, 0.4 mL) at 300 K with a Bruker AVANCE AQS600 spectrometer operating at the proton frequency of 600.13 MHz and equipped with a Bruker multinuclear z-gradient inverse probehead capable of producing gradients in the z direction with a strength of 55 G cm^{-1}. The ^{1}H NMR spectra were obtained using 32K data points, a recycle delay of 8 s, and a 90° flip angle pulse of 9 μs. The ^{1}H−^{1}H gradient-selected COSY-45 experiments were recorded using the following acquisition and processing parameters: a spectral width of 12 ppm in both dimensions, 4096 data points in the f2 dimension, 256 increments in the f1 dimension, a relaxation delay of 2 s, 16 dummy scans. and 200 scans. Data were processed in magnitude mode with 8192 × 1024 data points. Chemical shifts were referred to the residual singlet proton (8.03 ppm) of DMF-d_7.

Computational Details. DFT calculations were performed with the scalar relativistic ZORA (zero-order regular approximation)[7] formalism employing the *Amsterdam Density Functional* (*ADF*) program, release 2006.01.[8] Geometry optimizations were carried out in the gas phase and in DMSO solution using the local density approximation functional of Vosko−Wilk−Nusair,[9] plus the generalized gradient approximation, employing Becke's[10] gradient approximation for exchange and Perdew's[11] for correlation (BP86). The ZORA DZP- and TZP-optimized basis sets included in the *ADF* program were used for the main-group element and Pd atoms, respectively. The cores (C, N, 1s; Cl, 1s-2p; Pd, 1s-3d) were kept frozen and described by optimized ZORA orbitals. The optimized structures were verified to correspond to local minima (all-positive harmonic frequencies) by frequency calculations. Single-point calculations were performed in both DMSO and DMF solution, using the DMSO-optimized geometries. In these calculations, the model Kohn–Sham exchange-correlation potential SAOP[12] was employed in conjunction with the all-electron ZORA DZP- and TZP-optimized basis sets for the main-group element and Pd atoms, respectively.

For simulation of the solvent effects, the "Conductor-like Screening Model" (COSMO),[13] as implemented in *ADF*,[14] was used.

Electrochemical Measurements. Cyclic voltammetry was performed with an EG&G model 173 potentiostat coupled to an EG&G model 175 universal programmer. Current–voltage curves were recorded on an EG&G Princeton Applied Research model R-0151 $X-Y$ recorder. A three-electrode system was used, consisting of a glassy carbon working electrode, a platinum counter electrode, and a saturated calomel reference electrode (SCE).

Thin-layer spectroelectrochemistry measurements were carried out at an optically transparent thin-layer platinum working electrode using a Hewlett-Packard model 8453 diode array spectrophotometer coupled with an EG&G model 173 universal programmer. Three solvents for electrochemical measurements, pyridine (99.9+%), DMSO (99.9+%), and DMF (99.8+%), were purchased from Sigma-Aldrich Co. and used without further purification. High-

(5) Altomare, A.; Burla, M. C.; Cavalli, M.; Cascarano, G.; Giacovazzo, C.; Guagliardi, A.; Moliterni, A. G. G.; Polidori, G.; Spagna, R. *J. Appl. Crystallogr.* **1999**, *32*, 115.
(6) Sheldrick, G. M. *SHELXL97, Program for crystal structure refinement*; University of Göttingen: Göttingen, Germany, 1997.
(7) (a) van Lenthe, E.; Baerends, E. J.; Snijders, J. G. *J. Chem. Phys.* **1993**, *99*, 4597. (b) van Lenthe, E.; Baerends, E. J.; Snijders, J. G. *J. Chem. Phys.* **1994**, *101*, 9783. (c) van Lenthe, E.; Ehlers, A. W.; Baerends, E. J. *J. Chem. Phys.* **1999**, *110*, 8543.
(8) (a) *ADF 2006.01*; SCM, Theoretical Chemistry, Vrije Universiteit, Amsterdam, The Netherlands, available from http://www.scm.com. (b) te Velde, G.; Bickelhaupt, F. M.; Baerends, E. J.; Fonseca Guerra, C.; van Gisbergen, S. J. A.; Snijders, J. G.; Ziegler, T. *J. Comput. Chem.* **2001**, *22*, 931.
(9) Vosko, S. H.; Wilk, L.; Nusair, M. *Can. J. Phys.* **1980**, *58*, 1200.
(10) Becke, A. *Phys. Rev. A* **1988**, *38*, 3098.
(11) Perdew, J. P. *Phys. Rev. B* **1986**, *33*, 8822.
(12) (a) Gritsenko, O. V.; Schipper, P. R. T.; Baerends, E. J. *Chem. Phys. Lett.* **1999**, *302*, 199. (b) Schipper, P. R. T.; Gritsenko, O. V.; van Gisbergen, S. J. A.; Baerends, E. J. *J. Chem. Phys.* **2000**, *112*, 1344.
(13) (a) Klamt, A.; Schürmann, G. *J. Chem. Soc., Perkin Trans.* **1993**, *2*, 799. (b) Klamt, A.; Jonas, V. *J. Chem. Phys.* **1996**, *105*, 9972.
(14) Pye, C. C.; Ziegler, T. *Theor. Chem. Acc.* **1999**, *101*, 396.

Table 1. UV–Visible Spectral Data [λ, nm (log ϵ)] of the Palladium(II) Species in Different Solvents

compound	solvent	λ, nm (log ϵ)				
		Soret region		Q-band region		
$[(PdCl_2)_4Py_8TPyzPzPd]^a$	CH_3CN	339 (4.77)	370sh (4.39)	570 (4.15)	602sh (4.15)	629 (4.90)
	DMSO	341 (5.02)	370sh (4.69)	575 (4.34)		636 (5.03)
$[Py_8TPyzPzPd]\cdot 6H_2O$	CH_2Cl_2	341 (5.07)	400sh (4.47)	570 (4.51)	604sh (4.51)	628 (5.33)
	py	343 (5.05)	380sh (4.68)	573 (4.53)	611sh (4.56)	633 (5.30)
$[Py_8TPyzPzPd]\cdot 10H_2O$	DMSO	340 (4.94)	380sh (4.58)	575 (4.32)		633 (4.95)
$[(2\text{-Mepy})_8TPyzPzPd]^{8+b}$	py	350 (5.11)		580 (4.36)		637 (4.92)
	DMSO	342 (5.04)	380sh (4.63)	577 (4.41)		638 (5.14)

[a] Clathrated water: $15H_2O$. [b] Monohydrated species neutralized by I^- ions.

purity N_2 from Trigas was used to deoxygenate the solution before each electrochemical and spectroelectrochemical experiment. Tetra-*n*-butylammonium perchlorate (TBAP, 99%) from Fluka Chemika Co. was used as the supporting electrolyte (0.1 M for cyclic voltammetry and 0.2 M for spectroelectrochemistry) and stored under vacuum at 40 °C prior to use.

Other Physical Measurements. IR spectra were recorded on a Perkin-Elmer 783 in the range 4000–200 cm^{-1} (KBr pellets). UV–visible solution spectra, other than those for spectroelectrochemistry (see above), were recorded with a Varian Cary 5E spectrometer. TGA was performed on a Stanton Redcroft model STA-781 analyzer under a N_2 atmosphere (0.5 L min^{-1}). Elemental analyses for C, H, and N were provided by the "Servizio di Microanalisi" at the Dipartimento di Chimica, Università "La Sapienza" (Rome), on an EA 1110 CHNS-O instrument. The ICP-PLASMA Pd analyses were performed on a Varian Vista MPX CCD simultaneous ICP-OES. MALDI-TOF mass spectra for $[Py_8TPyzPzPd]$ in CH_2Cl_2 and CH_3CN solutions for $[(CN)_2Py_2PyzPdCl_2]$ and $[(PdCl_2)_4Py_8TPyzPzPd]$ were recorded with a Voyager DE STR instrument.

Results and Discussion

Synthesis and General Properties. The initial target of this study was preparation of the monopalladated species $[Py_8TPyzPzPd]$. Using standard procedures, the free-base macrocycle, $[Py_8TPyzPzH_2]$, was mixed with $PdCl_2$ in DMSO by using different molar ratios of the two reactants. The 1:1 molar ratio led always to an incomplete conversion of the unmetalated species into its corresponding metal derivative. When using a molar excess of $PdCl_2$ that was 2 or 3 times the number of moles of the free-base macrocycle, the products obtained always contained an excess of palladium(II) with respect to that expected for the monometalated species, thus suggesting that a mixture of macrocycles with a different number of Pd^{II} groups had been formed. However, the use of a larger molar ratio, i.e. $PdCl_2$/free base > 6:1, led systematically and reproducibly to the formation of a single porphyrazine product, which was identified as the hydrated pentapalladated species $[(PdCl_2)_4Py_8TPyzPzPd]$, as reported in the Experimental Section. Retention of clathrated water molecules by the solid material is a known feature for porphyrazine macrocycles and has been observed for related compounds with peripherally annulated heterocyclic rings like pyridine, thia/selenodiazole, or pyrazine.[1a,15] The clathrated water is normally eliminated by heating under vacuum at mild temperatures, but it is again at least partly recovered by exposure to the atmosphere. The number of retained water molecules was often different from preparation to preparation of each investigated palladium(II) species, but the number of water molecules on a given isolated product did not seem to affect the physicochemical properties of the examined species, and bound H_2O is therefore not indicated in the formulations given below.

The penta- and monopalladated species, $[(PdCl_2)_4Py_8TPyzPzPd]$, $[Py_8TPyzPzPd]$, and $[(2\text{-Mepy})_8TPyzPzPd]^{8+}$, are all air-stable dark-green materials, which exist as hydrated species in the solid state. A noteworthy feature in the IR spectrum of $[(PdCl_2)_4Py_8TPyzPzPd]$ is the presence of the stretching of the Pd−Cl bond as a moderately intense split absorption with peaks at 349 and 341 cm^{-1} (a similar split absorption with peaks at 340 and 335 cm^{-1} is found for the palladated precursor $[(CN)_2Py_2PyzPdCl_2]$). Absorptions at 993, 972, 790, 744, and 716 cm^{-1}, found present in the IR spectrum of $[Py_8TPyzPzPd]$, were also observed in the IR spectra of $[Py_8TPyzPzM]$ analogues,[1c] thus indicating that they are characteristic of peripherally unmetalated pyridinopyrazineporphyrazines. Actually, these absorptions were of some utility in discriminating the monopalladated complex from the pentapalladated species during the synthetic procedures. The IR spectrum of the octacation $[(2\text{-Mepy})_8TPyzPzPd]^{8+}$ does not differ significantly from that of the neutral parent in the 1600–400 cm^{-1} region, apart from the presence of a weak-to-medium intensity peak at 945 cm^{-1}.

Of the three synthesized palladium(II) complexes, only the iodide salt of the octacation $[(2\text{-Mepy})_8TPyzPzPd]^{8+}$ shows some (poor) solubility in water. All three complexes are generally insoluble or only slightly soluble in nonaqueous nondonor or low-donor solvents. Stable solutions of the pentapalladated species $[(PdCl_2)_4Py_8TPyzPzPd]$ are formed at ca. 10^{-5} M concentration in DMSO and CH_3CN, and the same is true for the monopalladated species $[Py_8TPyzPzPd]$ in pyridine, CH_2Cl_2, or DMSO, as well as for the iodide salt of the octacation $[(2\text{-Mepy})_8TPyzPzPd]^{8+}$ in pyridine or DMSO. Solutions of the three complexes in the above solvents are stable for at least a few hours, as verified by their unchanged UV–visible spectrum as a function of time. A summary of the UV–visible spectral data in the different

(15) (a) Stuzhin, P. A.; Ercolani, C. *The Porphyrin Handbook*; Kadish, K. M., Smith, K. M., Guilard, R., Eds.; Academic Press: New York, 2003; Vol. 15, Chapter 101, pp 263–364. (b) Kudrevich, S. V.; van Lier, J. E. *Coord. Chem. Rev.* **1996**, *156*, 163–182.

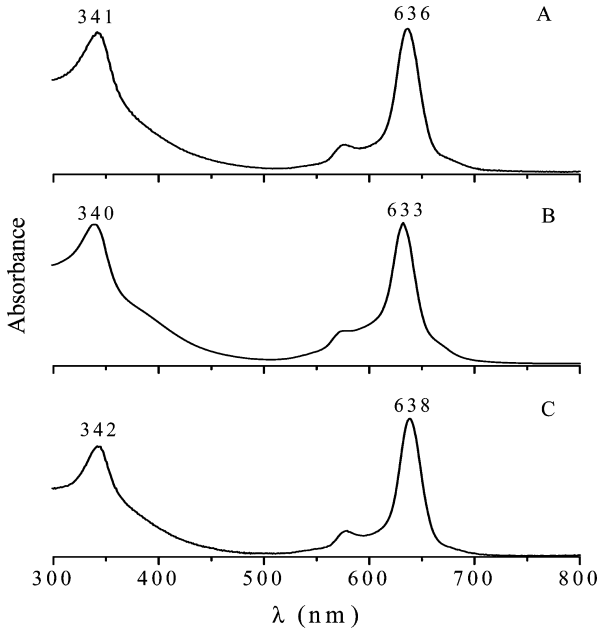

Figure 1. UV–visible spectra (c = ca. 10^{-5} M) in DMSO of (A) $[(PdCl_2)_4Py_8TPyzPzPd]$, (B) $[Py_8TPyzPzPd]$, and (C) $[(2\text{-}Mepy)_8TPyzPzPd]^{8+}$.

solvents is given in Table 1, and examples of spectra in DMSO are shown in Figure 1. The spectra of all three compounds are similar and have a pattern of the type normally observed for porphyrazine systems, with Soret and Q bands at 340–350 and 630–640 nm, respectively, due to intraligand $\pi-\pi^*$ transitions. The presence of a narrow Q band, accompanied by vibronic satellites and the absence of other absorptions in the range 500–800 nm, indicates that the compounds in these solvents are cleanly monomeric in the absence of detectable aggregation, although aggregation can often be observed for the monopalladated complex, as indicated by the appearance of an absorption at 660–670 nm, with aggregation being more heavily present at a concentration of ca. 10^{-4} M or higher. Similar spectra were obtained in DMF, but $[Py_8TPyzPzPd]$ showed an increased tendency toward aggregation and $[(PdCl_2)_4Py_8TPyzPzPd]$ showed a decreased stability at low concentrations. This is discussed on the following pages and will be further discussed in a forthcoming paper.[3]

Structural Characterization of the Pentanuclear Complex $[(PdCl_2)_4Py_8TPyzPzPd]$. Attempts to prepare single crystals of $[(PdCl_2)_4Py_8TPyzPzPd]$ suitable for X-ray investigation were unsuccessful because of the compound's low solubility, its tendency to clathrate water molecules, and the possible coexistence of structural isomers (see below). Insights into the structural features of the complex were instead derived from one- and two-dimensional ^{1}H NMR spectra in solution, DFT calculations, X-ray data, and solution ^{1}H NMR spectra of the $[(CN)_2Py_2PyzPdCl_2]$ precursor. A key aspect of the $[(PdCl_2)_4Py_8TPyzPzPd]$ structural characterization was to elucidate the type of coordination of the $PdCl_2$ groups to the external dipyridinopyrazine fragments. It is known from the literature that the dipyridinopyrazine fragment, which is present in 2,3-di-2-pyridylpyrazine (Chart 1A, R = H) and in its dicyano derivative

Chart 1

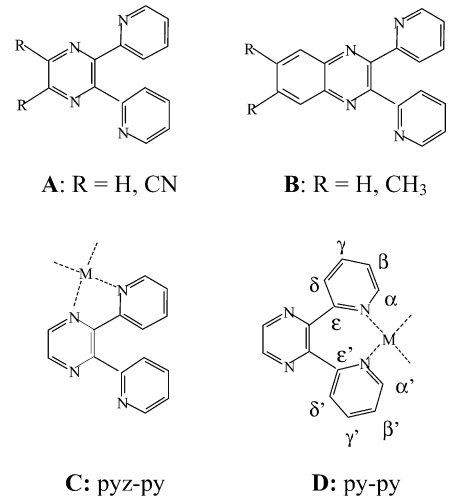

$[(CN)_2Py_2Pyz]$ (Chart 1A, R = CN) as well as in 2,3-di-2-pyridylquinoxaline and its derivatives substituted in the 6 and 7 positions (Chart 1B), can exhibit two different modes of coordination to metal ions. One mode involves the N atoms of vicinal pyrazine and pyridine rings, and the other mode involves the N atoms of two adjacent pyridine rings. These coordination modes are shown in parts C and D of Chart 1 and are denoted as pyz−py and py−py, respectively.

The pyz−py mode of coordination (Chart 1C) has been shown to occur in discrete mononuclear ruthenium(II)[16] and cobalt(II) complexes,[17] as well as in dinuclear 2:1 metal-to-ligand copper(II) complexes,[18] in one-dimensional copper(II)[19a] and molecular one- and two-dimensional copper(I) systems,[19b] with the pyridine and pyrazine rings of the chelate moiety approaching in all cases a nearly coplanar arrangement.

The dipyridinopyrazine fragment shows a py−py mode of coordination for binding to copper(II),[20] nickel(II),[21] and rhenium(V),[22] thus forming a seven-membered ring as illustrated in Chart 1D. In addition, both pyz−py and py−py coordination modes have been shown to exist within the same discrete unit of a 1:2 copper(II)/ligand complex.[23] To our knowledge, the only structurally characterized species where the dipyridinopyrazine fragment coordinates to palladium(II) is the dichloro[6,7-dimethyl-2,3-di-2-pyridyl-N-quinoxaline]-palladium(II) complex.[24] In this complex, the dipyridinopyrazine fragment coordinates the Pd^{II} ion in a py−py fashion,

(16) Rillema, D. P.; Taghdiri, D. G.; Jones, D. S.; Keller, C. D.; Worl, L. A.; Meyer, T. J.; Levy, H. A. *Inorg. Chem.* **1987**, *26*, 578.
(17) Escuer, A.; Vicente, R.; Comas, T.; Ribas, J.; Gomez, M.; Solans, X.; Gatteschi, D.; Zanchini, C. *Inorg. Chim. Acta* **1991**, *181*, 51.
(18) Gordon, K. C.; Al-Obaidi, Ala H. R.; Jayaweera, P. M.; McGarvey, J. J.; Malone, J. F.; Bell, S. E. J. *J. Chem. Soc., Dalton Trans.* **1996**, 1591.
(19) (a) Rarig, R. S. , Jr.; Hagrman, P. J.; Zubieta, J. *Solid State Sci.* **2002**, *4*, 77. (b) Chesnut, D. J.; Kusnetzov, A.; Birge, R. R.; Zubieta, J. *Inorg. Chem.* **1999**, *38*, 2663.
(20) Escuer, A.; Comas, T.; Ribas, J.; Vicente, R.; Solans, X.; Zanchini, C.; Gatteschi, D. *Inorg. Chim. Acta* **1989**, *162*, 97.
(21) Escuer, A.; Vicente, R.; Comas, T.; Ribas, J.; Gomez, M.; Solans, X. *Inorg. Chim. Acta* **1990**, *77*, 161.
(22) Bandoli, G.; Gerber, T. I. A.; Jacobs, R.; du Preez, J. G. H. *Inorg. Chem.* **1994**, *33*, 178.
(23) Goodwin, K. V.; Pennington, W. T.; Petersen, J. D. *Acta Crystallogr.* **1990**, *C46*, 898.

Table 2. Experimental Data for the X-ray Diffraction Study on Crystalline $[(CN)_2Py_2PyzPdCl_2]$

compound	$[(CN)_2Py_2PyzPdCl_2]$
formula	$C_{16}H_8Cl_2N_6Pd \cdot 0.75C_2H_3N$
a, Å	11.618(2)
b, Å	13.123(2)
c, Å	28.273(3)
β, deg	100.606(4)
V, Å^3	4236.9(11)
Z	8
fw	492.4
space group	$P2_1/c$
T, °C	20
λ, Å	0.710 73
ρ_{calc}, g cm^{-3}	1.544
μ, mm^{-1}	1.143
transmn coeff	0.856–0.966
R1[a]	0.063
wR2	0.095
GOF	0.743
N-observed[b]	2094
N-independent[c]	7841
N-refinement[d]	7841
variables	559

[a] Calculated on the observed reflections having $I > 2\sigma(I)$. [b] N-observed is the number of the independent reflections having $I > 2\sigma(I)$. [c] N-independent is the number of independent reflections. [d] N-refinement is the number of reflection used in the refinement having $I > 0$.

resulting in a square-planar N_2PdCl_2 moiety, just as observed in two platinum(II) analogues.[25]

Crystal data on the palladated precursor $[(CN)_2Py_2PyzPdCl_2]$ point to a py−py coordination mode of the dipyridinopyrazine fragment to Pd^{II}. The unit cell of $[(CN)_2Py_2PyzPdCl_2]$ contains two independent molecules (A and B; see Table 2). ORTEP views of molecules A and B are shown in Figure 2 and Figure S1 in the Supporting Information, respectively. As a result of the py−py coordination mode adopted by Pd^{II}, the pyridine rings within each dipyridinopyrazine fragment are oriented nearly orthogonally to each other, with dihedral angles of 89.4(4) and 83.2(4)° for N5/C7−C11 ^ N6/C12−C16 (Figure 2) and N11/C23−C27 ^ N12/C28−C32 (Figure S1 in the Supporting Information), respectively. The dihedral angles they form with the respective pyrazine rings range from 50.0(4) to 64.8(3)° (Table S2 in the Supporting Information). Selected bond distances and angles within the N_2PdCl_2 cores are listed in Table 3. The trends of the bond distances within the pyrazine rings are consistent with a complete delocalization of the double bond system. The palladium centers in the N_2PdCl_2 cores display a slightly distorted square-planar geometry [maximum deviations 0.056(10) and 0.023(14) Å for N6 and N12]. The Pd−N [mean value 2.04(2) Å] and Pd−Cl [mean value 2.279(5) Å] bond lengths are in good agreement with the mean values of 2.017(13) and 2.294(15) Å found in the Cambridge Crystallographic Databank for 68 and 290 entries, respectively. It is worth noting that N_2PdCl_2 is nearly perpendicular to the plane of the pyrazine core in molecule A (Figure 2, side view, 78.3(2)°; 85.3(1)° in molecule B).

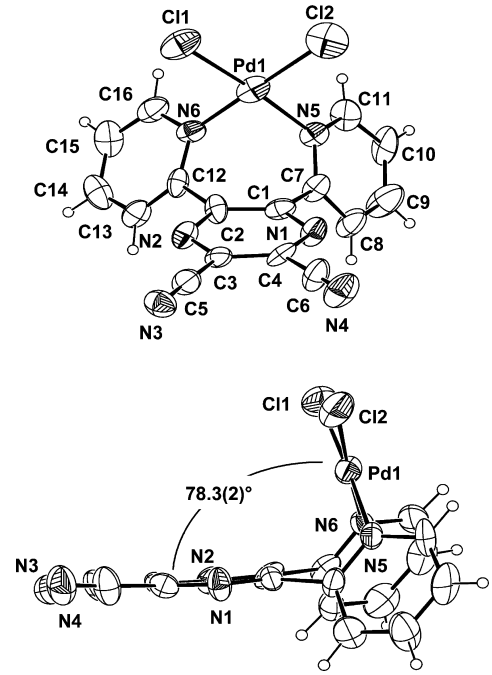

Figure 2. ORTEP front (top) and side (bottom) views (30% probability ellipsoids) of molecule A in $[(CN)_2Py_2PyzPdCl_2]$.

Table 3. Selected Bond Distances (Å) and Angles (deg) for $[(CN)_2Py_2PyzPdCl_2]$

complex molecule A		complex molecule B	
Pd1−N5	2.039(8)	Pd2−N11	2.046(8)
Pd1−N6	1.960(9)	Pd2−N12	2.083(8)
Pd1−Cl1	2.277(3)	Pd2−Cl3	2.270(3)
Pd1−Cl2	2.268(3)	Pd2−Cl4	2.289(2)
N6−Pd1−N5	86.8(3)	N11−Pd2−N12	86.7(3)
N6−Pd1−Cl2	177.3(2)	N11−Pd2−Cl3	178.1(2)
N5−Pd1−Cl2	91.1(3)	N12−Pd2−Cl3	91.4(3)
N6−Pd1−Cl1	89.8(3)	N11−Pd2−Cl4	90.0(2)
N5−Pd1−Cl1	175.8(3)	N12−Pd2−Cl4	176.6(2)
Cl2−Pd1−Cl1	92.35(12)	Cl3−Pd2−Cl4	91.87(10)

To ascertain whether the py−py coordination mode adopted by the $PdCl_2$ fragment in the palladated precursor $[(CN)_2Py_2PyzPdCl_2]$ is retained in the $[(PdCl_2)_4Py_8TPyzPzPd]$ complex, ^{1}H NMR measurements were made in DMF-d_7 solutions, on both complexes, and, for comparison purposes, on the unmetalated precursor $[(CN)_2Py_2Pyz]$. The ^{1}H NMR spectra of these three species in DMF-d_7 are shown in Figure 3, while a summary of the spectral data and related assignments are given in Table 4. A complete assignment of the α-, β-, γ-, and δ-type H atoms of the pyridine rings required ^{1}H−^{1}H COSY experiments to identify the resonance peak of the β proton (Figure 4), which was hidden by the amidic proton of DMF. Before the ^{1}H NMR results are discussed, it should be noted that 10^{-4} M (or possibly higher) solutions of the pentapalladated complex in DMF-d_7 are stable and show a ^{1}H NMR signal pattern typical of a monomeric species.

Only one set of four resonance peaks is associated with the H atoms of the pyridine rings of all of the three species (see Figures 3 and 4 and Table 4), which indicates that the pyridine rings are equivalent in each compound. This is as

(24) Nicolò, F.; Cusumano, M.; Di Pietro, M. L.; Scopelliti, R.; Bruno, G. *Acta Crystallogr.* **1988**, *C54*, 485.
(25) (a) Granifo, J.; Vargas, M. E.; Garland, M. T.; Baggio, R. *Inorg. Chim. Acta* **2000**, *305*, 143. (b) Granifo, J.; Vargas, M. E.; Rocha, H.; Garland, M. T.; Baggio, R. *Inorg. Chim. Acta* **2001**, *321*, 209.

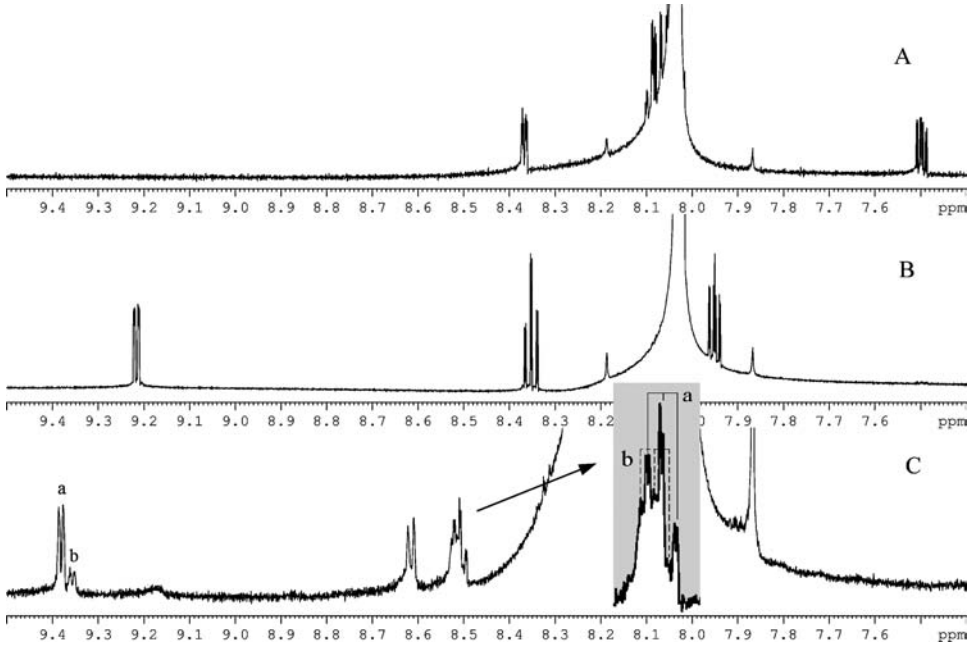

Figure 3. ^{1}H NMR spectra of (A) $[(CN)_2Py_2Pyz]$, (B) $[(CN)_2Py_2PyzPdCl_2]$, and (C) the pentapalladated species $[(PdCl_2)_4Py_8TPyzPzPd]$ (a, major component; b, minor component). The inset in part C helps in the reading of the a and b components.

Table 4. ^{1}H NMR Parameters for the Species $[(CN)_2Py_2Pyz]$, $[(CN)_2Py_2PyzPdCl_2]$ and the Pentapalladated Species $[(PdCl_2)_4Py_8TPyzPzPd]$

	$[(CN)_2Py_2Pyz]$			$[(CN)_2Py_2PyzPdCl_2]$			$[(PdCl_2)_4Py_8TPyzPzPd]$		
	^{1}H (ppm)	m	*J* (Hz)	^{1}H (ppm)	m	*J* (Hz)	^{1}H (ppm)	m	*J* (Hz)
α	8.367	ddd	4.7, 1.6, 1.4	9.216	dd	5.7, 1.5	9.382 a[a]	bd[d]	6.6
							9.357 b[b]	bd[d]	6.6 6.6
β	7.497	ddd	4.7, 7.1, 1.6	7.950	ddd	5.7, 7.7, 1.5	8.047 a[a]	H[e]	
							8.051 b[b]	H[e]	
γ	8.068	ddd	7.1, 7.6, 1.8	8.352	ddd	7.7, 7.7, 1.5	8.507 a[a,c]	ddd	7.9, 7.9, 1.8
							8.514 b[b,c]	ddd	7.1, 7.1, 1.0
δ	8.093	ddd	7.6, 1.6, 1.3	8.027	h[b]		8.615	bd[d]	7.4

[a] a = major component. [b] b = minor component. [c] Resonance peaks evidenced in the inset of Figure 3C. [d] bd = broad doublet. [e] h = hidden: the assignment was obtained by means of an ^{1}H−^{1}H COSY experiment.

expected for the metal-free $[(CN)_2Py_2Pyz]$ fragment for which an earlier ^{1}H NMR[1b] study in $CDCl_3$ indicated the equivalence of the pyridine rings, as well as for the palladated complex $[(CN)_2Py_2PyzPdCl_2]$, in which both pyridine rings of the dipyridinopyrazine fragment are, according to X-ray data, involved through their N atoms in a coordination to $PdCl_2$. Most importantly, the presence of only one set of resonance peaks in the ^{1}H NMR spectrum of the pentanuclear palladium(II) complex (indicated as form a in Figure 3C) is only consistent with a py−py type of coordination. If indeed only one of the two pyridine rings belonging to a dipyridinopyrazine fragment was coordinated to the metal, two distinct sets of four resonance peaks in the aromatic region of the NMR spectrum would be detected.

A good reference for this type of nonequivalent pyridine ring is given by the complex $[(dhp)PtCl_2]$ (dhp = 2,3-di-2-pyridyl-5,6-dihydropyrazine)[25b] in which Pt^{II} is coordinated in the pyz−py fashion (Chart 1C). Because of the nonequivalence of the two pyridine rings in this complex, the ^{1}H NMR spectrum exhibits a pattern in which the resonance peaks are doubled, with one set of four peaks assigned to the pyridine ring coordinated to Pt^{II} and the other set of four peaks to the free pyridine ring.

Looking at the chemical shifts listed in Table 4, it is apparent that in going from the precursor (Figure 3A) to its monopalladated complex (Figure 3B) a remarkable low-field shift is observed for three of the four resonance peaks (α,α′, 8.367 → 9.216; *β*,*β*′, 7.497 → 7.950; *γ*,*γ*′, 8.068 → 8.352), while the fourth one shows a small change in the reverse direction (*δ*,*δ*′, 8.093 → 8.027; this latter value might be somewhat affected by the hiding effect of the solvent). In keeping with expectation, the highest shift is observed for the α proton, which is the one closest to the coordinated N atom (Chart 1D). The *π*-ring current associated with macrocyclization induces a further low-field shift of all of the four resonance peaks, as inferred from the chemical shift values reported in Table 4 for the pentapalladated complex and its metal-free and monopalladated precursors. While the downfield shift for the α, *β*, and *γ* protons is small (0.10–0.15 ppm), the shift for the *δ* proton, which is the closest to the *π*-ring framework, is quite large (0.6 ppm). Notably, previous ^{1}H NMR studies on the metal-free precursor, $[(CN)_2Py_2Pyz]$, and the free-base macrocycle, $[Py_8PyzPzH_2]$, revealed a similar macrocyclization-induced downfield shift of the pyridine proton resonances.[1b] The ^{1}H NMR spectrum of the pentapalladated species (Figure 3C) also shows the presence

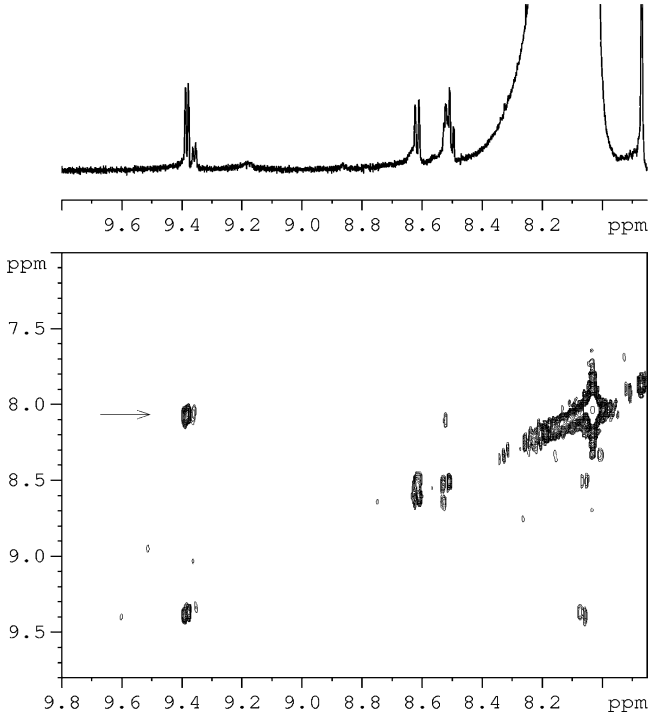

Figure 4. $^1H-^1H$ COSY map of $[(PdCl_2)_4Py_8TPyzPzPd]$ in DMF-d_7 at 300 K. The cross peak between the α and β protons is indicated by the arrow.

Scheme 2. Structural Isomers Generated by the Arrangement of the Dipyridino-$PdCl_2$ Fragments in the Pentapalladated Species

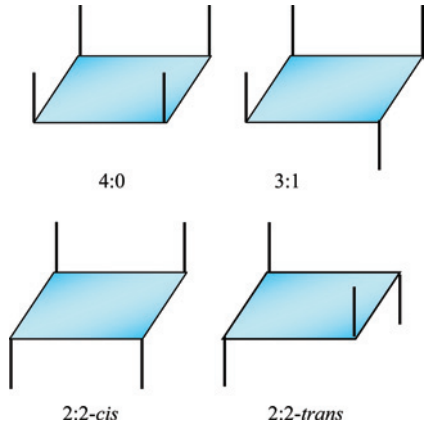

of a minority form (b) of the compound with slightly different chemical shifts as compared to those of form a, and extremely close J values are calculated for two of the four resonance peaks (see Table 4).

The presence of only one prevalent set of four resonance peaks in the ^1H NMR spectrum of the pentapalladated species not only unequivocally establishes a py−py coordination mode of the peripheral $PdCl_2$ fragments but also indicates that the eight pyridines are equivalent on the NMR time scale in both forms a and b of the complex.

This implies that, depending on the relative arrangement of the peripheral N_2PdCl_2 moieties with respect to the porphyrazine plane, among the four structural isomers (Scheme 2) that are likely to be formed during cyclotetramerization of the metal-free precursor in the presence of $PdCl_2$, only the 4:0, 2:2-cis, and 2:2-trans are, in principle, compatible with the NMR spectral features.

In order to gain insight into the actual conformation of the dominant and minority forms (a and b) detected by the NMR spectra, the geometry and relative energy of the 4:0, 2:2-cis, and 2:2-trans isomers were theoretically investigated. Initially, their geometries were optimized in the gas phase without symmetry constraints. The crystallographic data of the monopalladated precursor were used to build up the peripheral fragments of the starting structures. Geometry optimization of the 4:0, 2:2-cis, and 2:2-trans forms afforded structures of C_{4v}, C_i, and D_{2d} symmetry, respectively. These structures were found to correspond to stable minima (all-positive harmonic frequencies).

Because the pentapalladated complex was assembled in a DMSO solution, the structures of the three possible isomers were reoptimized in this solvent under C_{4v} (4:0), C_i (2:2-cis), and D_{2d} (2:2-trans) symmetry constraints. The relative energies and the most relevant structural parameters computed in the gas phase and in DMSO solution are summarized in Table 5, whereas their DMSO-optimized structures are displayed in Figure 5.

In the gas phase, the lowest energy was found for the slightly saddled **1a** form with D_{2d} symmetry, with the **1b** and **1c** forms being 10.0 and 39.0 kJ mol^{-1} less stable, respectively. The relative energies of the **1a**−**1c** forms change in the condensed phase, where **1a** and **1b** are found to be less stable than **1c** by 6.0 and 7.0 kJ mol^{-1}, respectively. The considerable stabilization of **1c** in DMSO fits in with the solvation energy computed for this isomer, being 119.7 and 89.0 kJ mol^{-1} larger than those for **1a** and **1b**, respectively. According to the relative energies of the three isomers in DMSO, the dominant form of the pentapalladated complex is likely to correspond to the **1c** isomer with C_{4v} symmetry. As for the minority form b, the nearly degenerate **1b** and **1a** isomers are both plausible candidates.

Analysis of the bond parameters computed for **1a**−**1c** reveals that the orientation of the peripheral fragments has only a minor impact, if any, on the geometry of the macrocycle as well as of the peripheral N_2PdCl_2 moieties, either in the gas phase or in solution. When the gas-phase and DMSO geometries are compared, it is apparent that the solvent, apart from inducing a modest shortening of the $Pd-N_p$ distance and contraction of the macrocycle ring, mostly affects the coordination sphere of the peripheral Pd^{II} centers. As inferred from the data in Table 5, inclusion of solvation effects causes a lengthening of the Pd−Cl bond by ca. 0.04 Å and a shortening of the $Pd-N_{py}$ bond by ca. 0.01 Å. In addition, from the gas phase to the DMSO solution, the bond angles defining the coordination sphere of the peripheral Pd^{II} centers approach closer to 90°. In general, the bond parameters of the peripheral N_2PdCl_2 moieties computed in DMSO are more in line with the X-ray data of the monopalladated precursor than those computed in the gas phase, with the only exception being the Pd−Cl bond, which is slightly overestimated in solution.

Table 5. Relative Energies and Selected Bond Parameters (Å, deg) of the **1a**−**1c** [$(PdCl_2)_4Py_8TPyzPzPd$] Structural Isomers

	1a D_{2d}		**1b** C_i		**1c** C_{4v}		
parameter[a]	gas phase	DMSO	gas phase	DMSO	gas phase	DMSO	exptl[b]
ΔE(kJ mol^{-1})	0.0	6.0	10.0	7.0	39.0	0.00	
Pd–N_p	1.993	1.990	1.994	1.991	1.999	1.991	
Pd–Cl	2.299	2.339	2.298	2.340	2.299	2.338	2.279(5)
Pd–N_{py}	2.067	2.049	2.068	2.050	2.070	2.050	2.04(2)
C_α–N_p	1.376	1.372	1.376	1.372	1.382	1.372	
C_α–C_β	1.458	1.457	1.458	1.457	1.463	1.456	
C_β–C_β	1.396	1.396	1.396	1.396	1.403	1.396	
C_α–N_b	1.318	1.319	1.318	1.319	1.322	1.319	
C_β–N_{pyz}	1.328	1.328	1.329	1.328	1.332	1.329	
C_{pyz}–C_{py}^{ϵ}	1.485	1.484	1.486	1.484	1.493	1.484	
C_α–N_p–C_α	110.7	110.6	110.7	110.6	110.6	110.6	
C_α–N_b–C_α	123.8	123.6	123.9	123.6	123.8	123.6	
N_{py}–Pd–N_{py}	89.3	86.7	89.3	87.4	89.2	86.6	86.8(3)
Cl–Pd–Cl	92.3	91.1	92.2	90.9	92.0	91.1	92.11(11)
N_{py}–Pd–Cl	89.1	91.1	89.1	90.8	89.2	91.1	90.6(3)
θ[c]	2.4	2.8	0.0	0.0	0.0	0.0	
ϕ[d]	57.5	57.5	57.8	57.1	57.5	58.7	57.4(4)

[a] For the C_i isomer, the average values of the geometrical parameters are reported. [b] Average X-ray values for the precursor of the pentapalladated complex, $[(CN)_2Py_2PyzPdCl_2]$, from this work. [c] θ is the C_α–N_p–N_p–C_α torsional angle of the adjacent pyrrole ring planes (saddling). [d] ϕ is the N_{py}–C^{ϵ}_{py}–C_{pyz}–C_{pyz} torsional angle, which provides a measure of the tilting of the pyridine ring plane with respect to the pyrazine ring plane.

Molecular Structure of the Mononuclear Complex [$Py_8TPyzPzPd$]. As in the case of the pentapalladated complex, attempts to prepare single crystals of the complex [$Py_8TPyzPzPd$] suitable for X-ray investigation were unsuccessful. To get information on the molecular structure of [$Py_8TPyzPzPd$], we turned to DFT calculations. The complex was expected to show a rich conformational behavior because different orientations of the pyridine rings can generate a number of conformers. However, X-ray data on the metal-free precursor, $[(CN)_2Py_2Pyz]$,[1b] indicate that the vicinal pyridine rings (those appended to the same pyrazine ring) tend to assume a preferential orientation, with the two pyridine rings tilted by ca. 38° relative to the pyrazine plane and the pyridine N atoms oriented oppositely. Thus, we focused on the energy and geometry of the four conformers of [$Py_8TPyzPzPd$] depicted in Scheme 3, wherein the N atoms of the vicinal pyridine rings have the same ud (u, up; d, down) orientation as that in the X-ray structure of the $[(CN)_2Py_2Pyz]$ precursor. Symmetry-constrained geometry optimizations of the four conformers were performed both in the gas phase and in DMSO. Because the C_4 and S_4 symmetries are not available in the *ADF* code, a C_2 symmetry constraint was used for **2a** and **2d**. The relative energies and the most relevant geometrical parameters computed for the **2a**−**2d** conformers are reported in Table 6. Calculated relative energies indicate that the nearly degenerate **2a** and **2b** conformers are the most stable, both in the gas phase and in solution, although the **2c** and **2d** conformers are not much higher in energy, particularly in DMSO. According to the data in Table 6, bond lengths and angles of the pyrazinoporphyrazine macrocycle are nearly insensitive to solvent effects and vary little from one conformer to another. This is not the case for the degree of distortion of the macrocycle. As can be inferred from the θ values in Table 6, the deviation from planarity of the porphyrazine core in **2c**, and even more in **2d**, is larger than that in **2a** and **2b**, particularly in the gas phase, where the ω and θ values are invariably larger than those in DMSO. That the most distorted conformers are also the less stable ones fits in with the scarce flexibility of the porphyrazine ring.

According to the calculated ϕ values, the degree of tilting of the pyridine ring plane with respect to the pyrazine ring plane ranges from 35.6 to 43.6°, depending on the conformer and phase. These values compare well with the average value of 38.7° determined for the metal-free precursor, $[(CN)_2Py_2Pyz]$, by X-ray studies.[1b] This suggests that the orientation of the pyridine rings observed in the precursor is dictated by intrinsic electronic factors such as the necessity to minimize the steric repulsion between the nitrogen lone pairs and the heterocycle π systems, while preserving an appreciable π conjugation with the pyrazine ring. The C_{pyz}–C^{ϵ}_{py} distance of ca. 1.48 Å experimentally observed in the precursor[1b] and predicted by DFT calculations for the [$Py_8TPyzPzPd$] conformers (see Table 6) is indeed a little shorter than that of typical C−C σ bonds (1.53 Å).[26]

Electronic Structure of [$Py_8TPyzPzPd$] and [$(PdCl_2)_4$-$Py_8TPyzPzPd$]. To provide insights into the energy and nature of the frontier orbitals controlling the electrochemical properties of the mono- and pentapalladated complexes, single-point calculations were performed. Although the very small energy gap ($\sim RT$ at room temperature) between the [$Py_8TPyzPzPd$] conformers makes them all accessible in a DMSO solution, we restricted the ground-state electronic structure analysis to the most stable conformer, **2b**. The nearly degenerate **2a**, **2c**, and **2d** conformers have very similar molecular structures, and their electronic structures are not expected to be significantly different from that of the **2b** conformer. As for the pentapalladated complex, we focused on the **1c** isomer, which is, according to NMR experiments and DFT calculations, the dominant form of [$(PdCl_2)_4Py_8TPyzPzPd$] in DMSO. Because the electrochemical experiments were conducted in DMSO and DMF, the single-point calculations were performed in both solvents. As it is fair to expect for solvents with comparable dielectric

(26) Allen, F. H.; Kennard, O.; Watson, D. G.; Brammer, L.; Orpen, A. G.; Taylor, R. *J. Chem. Soc., Perkin Trans.* **1987**, *2*, S1.

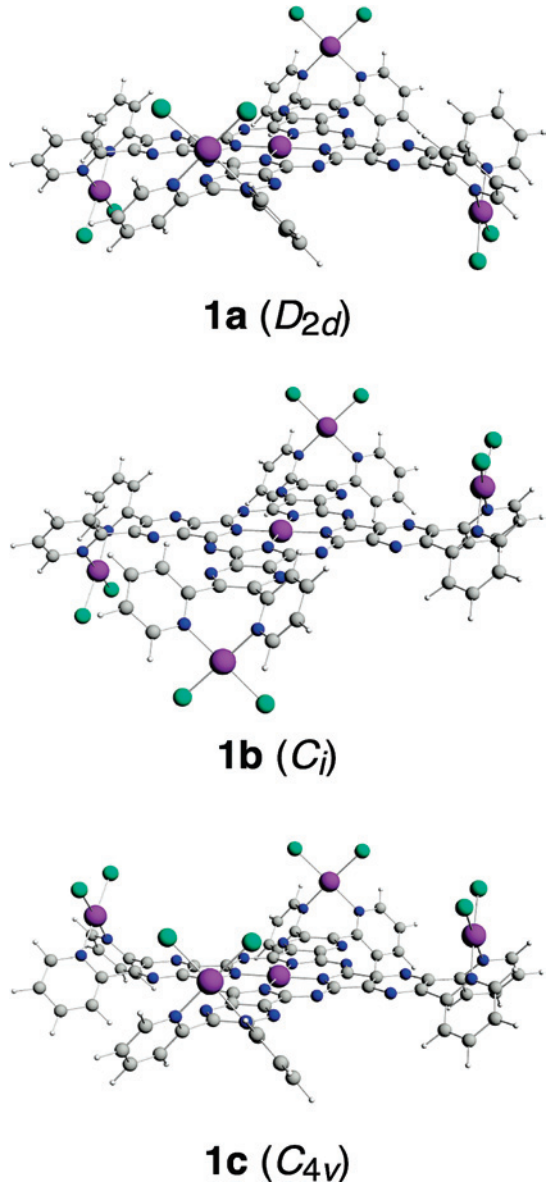

Figure 5. DMSO-optimized geometries of the 2:2-trans (**1a**), 2:2-cis (**1b**), and 4:0 (**1c**) structural isomers of $[(PdCl_2)_4Py_8TPyzPzPd]$.

constants ($\epsilon_{DMSO} = 46.7$; $\epsilon_{DMF} = 39.3$), the energy and composition of the molecular orbitals (MOs) are substantially the same in the two solvents. Therefore, only the DMSO results are discussed in the following.

The highest occupied (HOMO) and lowest unoccupied (LUMO) ground-state one-electron levels calculated for **2b** and **1c** are shown in Figure 6, where plots of selected molecular orbitals are also displayed.

We concentrate first on the theoretical results obtained for the monopalladated complex and later point out the effects of the peripherally coordinated $PdCl_2$ fragments. As inferred from the plots of Figure 6, the HOMO and the two nearly degenerate LUMOs of $[Py_8TPyzPzPd]$ are basically π orbitals of the pyrazinoporphyrazine macrocycle, with Pd $4d_\pi$ contributing to the latter by only 3%. Notably, in these MOs, one may recognize the well-known Gouterman HOMOs and LUMOs of Pcs, with the contribution of the benzo ring C_{ortho} $2p_z$ being simply replaced by the pyrazine ring N_{pyz} $2p_z$. However, because of the stabilizing effect of

Scheme 3. Conformers of $[Py_8TPyzPzPd]$, wherein the N atoms of the vicinal pyridine rings have the same orientation (ud) as those in the X-ray structure of the $[(CN)_2Py_2Pyz]$ precursor

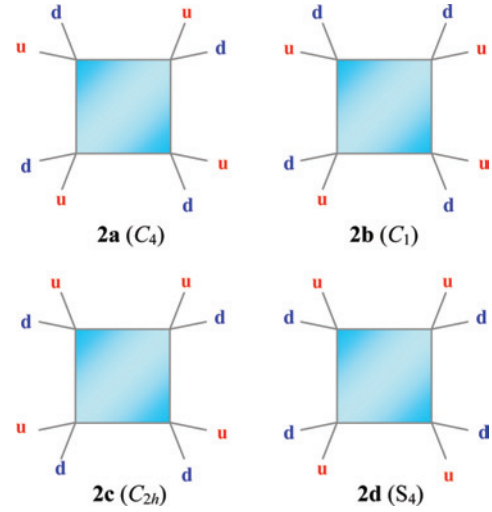

the pyrazine and pyridine rings, the HOMOs and LUMOs of the monopalladated complex are significantly downward shifted with respect to the [PcPd] counterparts. According to our calculations, upon going from [PcPd] to $[Py_8TPyzPzPd]$, the HOMOs and LUMOs are stabilized by 0.8 and 0.6 eV, respectively. This is in line with electrochemical data showing that the monopalladated complex as well as its copper(II) and zinc(II) analogues undergoes more facile stepwise reductions and more difficult oxidations as compared to the corresponding Pc complexes. The HOMO of the monopalladated complex is followed, in order of decreasing energy, by a set of π MOs mostly localized on the pyridine and pyrazine rings, the highest two of which are reported in the diagram of Figure 6. A quite large energy gap (ca. 1 eV) separates the LUMOs from a set of five closely spaced π MOs, which have a large amplitude on the pyrazinoporphyrazine macrocycle, as is evident from the representative plot of Figure 6. It is worth noting that no metal state enters the diagram of Figure 6 save for the Pd $4d_{x^2-y^2}$, which is pushed up by σ antibonding with the pyrrolic nitrogen lone pairs. The pertinent σ^*_{Pd-Np} MO lies in the virtual spectrum of $[Py_8TPyzPzPd]$ at -7.0 eV, at much higher energy than the LUMOs. Of the occupied Pd 4d orbitals, the $4d_{z^2}$ and $4d_{xy}$ are almost pure metal states, while the $4d_\pi$ heavily mixes with the N_p $2p_z$. All of the occupied metal states are located at too low energy to enter the diagram of Figure 6 (the $4d_{z^2}$, which is the highest in energy, is located at -11.0 eV).

Moving now to the pentapalladated complex, the diagram of Figure 6 shows that the peripheral electron-withdrawing $PdCl_2$ groups cause a significant stabilization of all $[Py_8TPyzPzPd]$ levels, particularly those with large amplitude on the pyrazine and pyridine rings. Actually, the set of MOs with π_{pyz-py} character is so much downshifted in the pentapalladated complex that it no longer enters the diagram of Figure 6. The electron-withdrawing effect of the $PdCl_2$ groups also manifests in a modest depletion of the electron density on the central Pd atom. Indeed, according to the Hirshfeld charge analysis, the central Pd atom carries a more

Table 6. Relative Energies and Selected Bond Parameters (Å, deg) of the DFT-Optimized [Py_8TPyzPzPd] Conformers

	2a C_4		**2b** C_1		**2c** C_{2h}		**2d** S_4	
parameter[a]	gas phase	DMSO	gas phase	DMSO	gas phase	DMSO	gas phase	DMSO
ΔE (kJ mol^{-1})	0.0	1.3	0.9	0.0	6.3	3.1	10.2	3.6
Pd–N_p	1.993	1.990	1.993	1.990	1.993	1.990	1.990	1.988
C_α–N_p	1.376	1.372	1.376	1.372	1.376	1.372	1.375	1.371
C_α	1.457	1.456	1.457	1.456	1.457	1.456	1.458	1.456
C_α	1.398	1.396	1.398	1.396	1.397	1.395	1.398	1.396
C_α–N_b	1.318	1.320	1.318	1.320	1.318	1.320	1.319	1.320
C_α–N_{pyz}	1.330	1.330	1.330	1.330	1.330	1.329	1.330	1.330
C_{pyz}–C^ϵ_{py}	1.480	1.481	1.480	1.481	1.481	1.482	1.482	1.482
$N_{py}\cdots N_{py}$	2.921	3.015	2.913	3.020	2.895	2.986	2.896	3.000
C_α–N_p–C_α	110.6	110.5	110.6	110.5	110.6	110.5	110.8	110.6
C_α–C_α	123.9	123.6	123.9	123.7	123.9	123.6	123.8	123.6
ω[b]	1.0	0.5	2.2	1.3	3.1	2.3	13.1	9.7
θ[c]	1.0	0.4	1.0	0.0	4.0	1.4	0.0	0.0
ϕ[d]	36.2	39.8	35.6	40.7	38.1	41.7	39.4	43.6

[a] Average values. [b] ω is the C_α–N_p–N_p–C_α torsional angle of the opposite pyrrole ring planes with respect to an axis through the pyrrolic N atoms (ruffling). [c] θ is the C_α–N_p–C_α torsional angle of the adjacent pyrrole ring planes (saddling). [d] ϕ is the N_{py}–C^ϵ_{py}–C_{pyz}–C_{pyz} torsional angle, which provides a measure of the tilting of the pyridine ring plane with respect to the pyrazine ring plane.

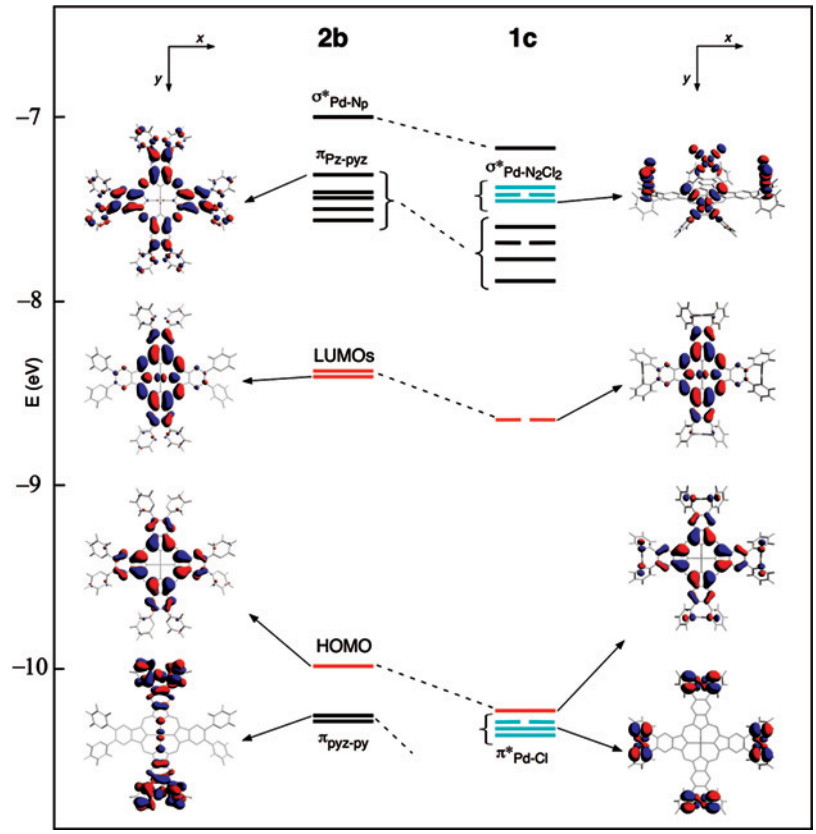

Figure 6. DFT-SAOP ground-state electronic structure of [Py_8TPyzPzPd] and [$(PdCl_2)_4Py_8$TPyzPzPd] in a DMSO solution. Also shown are isodensity surface plots of selected MOs.

positive charge in [$(PdCl_2)_4Py_8$TPyzPzPd] than in [Py_8TPyzPzPd] (+0.51 vs +0.49).

As inferred from the diagram of Figure 6, the frontier orbitals of [$(PdCl_2)_4Py_8$TPyzPzPd] also comprise MOs localized on the peripheral N_2PdCl_2 moieties. Immediately below the HOMO, there is a set of MOs with Pd $4d_\pi$ Cl−lone pair π-antibonding character. In the virtual spectrum, just above the π_{pz-pyz} set, we locate four nearly degenerate MOs with σ-antibonding character between the Pd $4d_{x^2-y^2}$ and the N_{py} and Cl lone pairs. These orbitals are likely to be involved in multielectron reduction processes at a potential more cathodic than that of the second one-electron reduction of the macrocycle ring (vide infra).

Electrochemistry. Cyclic voltammetry and spectroelectrochemistry of the three palladium(II) porphyrazines and $PdCl_2$ were carried out in three different solvents (pyridine, DMSO and DMF), all containing 0.1 M TBAP. The results of these studies are discussed below.

[Py_8TPyzPzPd]. At the concentrations used for the electrochemical experiments (ca. 5×10^{-4} M or higher), [Py_8TPyzPzPd] is present as an aggregate in the utilized nonaqueous solvents, but aggregation is broken up upon formation of the porphyrazine dianion, trianion, or tetranion under application of the appropriate reducing potential. This is illustrated in Figure 7 which shows cyclic voltammograms of [Py_8TPyzPzPd] on the first potential scan from 0.00 to

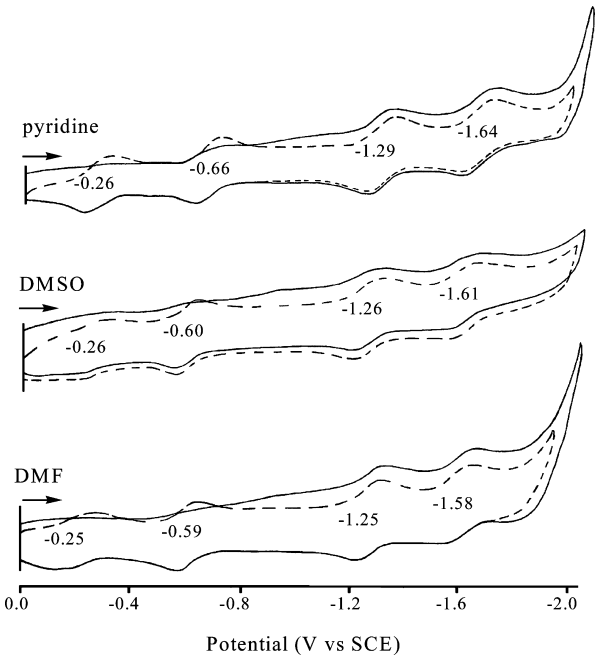

Figure 7. Cyclic voltammograms with added $E_{1/2}$ values (V vs SCE) of [Py_8TPyzPzPd] in pyridine, DMSO, and DMF containing 0.1 M TBAP. Scan rate = 0.1 V/s (— first scan; - - - second scan).

−2.0 V where the porphyrazine is aggregated (solid line), and on the second scan over the same potential range where the compound exists as a monomer (dashed line). As seen in the figure, the first two reductions of aggregated [Py_8TPyzPzPd] cannot be observed by cyclic voltammetry in any of the three utilized nonaqueous solvents, but the third and fourth reductions on the first potential sweep are well-defined and occur in the range of −1.25 to −1.29 V for [Py_8TPyzPzPd]$^{2-/3-}$ and −1.58 to −1.64 V for [Py_8TPyzPzPd]$^{3-/4-}$.

The fact that well-defined reductions are seen only for the last two processes of [Py_8TPyzPzPd] is because the initial sweep to negative potentials breaks up aggregation at the electrode surface upon formation of the doubly reduced porphyrazine, and four diffusion-controlled (re)oxidation processes can then be observed upon reversal of the potential sweep at −2.0 V and return to 0.00 V. Each reoxidation peak on the return scan corresponds to a one-electron transfer starting from the porphyrazine tetraanion, and the totally reoxidized compound corresponds to monomeric [Py_8TPyzPzPd] upon reaching a potential of 0.00 V. The neutral monomer formed in solution after reduction and reoxidation can then be reversibly reduced in four one-electron steps prior to the reformation of aggregates on longer time scales.

The stability of the monomeric form of [Py_8TPyzPzPd] generated after the initial potential sweep from 0.00 to −2.0 V varies with the specific solvent (py, DMSO, or DMF) and compound concentration (which ranged from 10^{-3} to 10^{-4} M), but at a scan rate of 0.10 V s^{-1}, well-defined current–voltage curves could always be obtained on the second, third, and all further potential sweeps; these gave in each case the same reproducible current–voltage curves and the same half-wave potentials for the four stepwise ligand-centered reductions of the neutral porphyrazine. The prevailing electrode reactions of monomeric [Py_8TPyzPzPd] are described by eqs 1–4, and the measured half-wave potentials are summarized in Table 7, which also includes data on earlier examined Py_8TPyzPz[1c] and (2-Mepy)$_8$TPyzPz derivatives.[1e]

Table 7. Half-Wave Potentials [a] for Reduction of the Investigated Compounds and Related Derivatives in Different Nonaqueous Solvents Containing 0.1 M TBAP

		macrocycle	centerreduction				$\Delta E_{1/2}$		
solvents	compound[b]	first	second	third	fourth	$PdCl_2$	Δ_{1-2}	Δ_{2-3}	Δ_{3-4}
py	[LPd]	−0.26	−0.66	−1.29	−1.64		0.40	0.63	0.35
	[$(PdCl_2)_4$LPd]	−0.26	−0.65	−1.27	−1.62	−0.85	0.39	0.62	0.35
	$PdCl_2$					−0.83			
	[L′Pd]$^{8+}$	0.07	−0.33				0.40		
	[LCo][c]	−0.26	−0.87	−1.37	−1.83		0.61	0.50	0.46
	[LCu][c]	−0.30	−0.68	−1.28	−1.61		0.38	0.61	0.33
	[LZn][c]	−0.34	−0.72	−1.38	−1.66		0.38	0.66	0.28
	[LMg(H_2O)][c]	−0.40	−0.79	−1.43	−1.70		0.39	0.64	0.28
DMSO	[LPd]	−0.26	−0.60	−1.26	−1.61		0.34	0.66	0.35
	[$(PdCl_2)_4$LPd]	0.00	−0.37	−1.24	−1.59	−0.98	0.37	0.87	0.35
	$PdCl_2$					−0.86			
	[L′Pd]$^{8+}$	0.08	−0.33				0.41		
	[LCo][c]	−0.06	−0.76	−1.31	−1.77		0.70	0.55	0.46
	[LCu][c]	−0.22	−0.58	−1.22	−1.58		0.36	0.64	0.36
	[LZn][c]	−0.26	−0.67	−1.38	−1.64		0.41	0.71	0.26
	[LMg(H_2O)][c]	−0.33	−0.70	−1.39	−1.67		0.37	0.69	0.28
	[L′Co]$^{8+}$ [d]	0.05	−0.51				0.56		
	[L′Cu]$^{8+}$ [d]	−0.04	−0.38				0.34		
	[L′Zn]$^{8+}$ [d]	−0.10	−0.44				0.34		
	[L′Mg(H_2O)]$^{8+}$ [d]	−0.19	−0.47				0.28		
DMF	[LPd]	−0.25[e]	−0.59	−1.25	−1.58		0.34	0.66	0.33
	[$(PdCl_2)_4$LPd]	0.04	−0.37	−1.27	−1.62	−1.03	0.41	0.90	0.35
	$PdCl_2$					−0.86			
	[L′Pd]$^{8+}$	0.12	−0.48				0.60		

[a] $E_{1/2}$ (V vs SCE). Scan rate of 0.1 V s^{-1}. [b] L = Py_8TPyzPz; L′ = (2-Mepy)$_8$TPyzPz. [c] Taken from ref 1c. [d] Taken from ref 1e. [e] A small peak can also be seen at −0.13 V. tw = this work.

$$[Py_8TPyzPzPd] + e^- \rightleftharpoons [Py_8TPyzPzPd]^- \quad (1)$$

$$[Py_8TPyzPzPd]^- + e^- \rightleftharpoons [Py_8TPyzPzPd]^{2-} \quad (2)$$

$$[Py_8TPyzPzPd]^{2-} + e^- \rightleftharpoons [Py_8TPyzPzPd]^{3-} \quad (3)$$

$$[Py_8TPyzPzPd]^{3-} + e^- \rightleftharpoons [Py_8TPyzPzPd]^{4-} \quad (4)$$

The maximum peak currents for all four reductions of [Py_8TPyzPzPd] in pyridine and the last three reductions of the compound in DMSO or DMF are almost identical (see Figure 7), consistent with an equal number of electrons being transferred in each process. The measured $E_{1/2}$ values for reduction of [Py_8TPyzPzPd] are also similar in the three solvents (see Table 7), although two forms of the neutral porphyrazine seem to be present on the second scan in DMSO and DMF, where the current–voltage curves show what appears to be two or more overlapping processes at closely spaced potentials. This could be due to different solvated forms of neutral [Py_8TPyzPzPd] but more likely results from a mixture of a monomer and aggregates in the DMSO and DMF solutions.

The electrochemistry of [Py_8TPyzPzPd] in pyridine most closely resembles that of [Py_8TPyzPzCo] with respect to the ease of the first reduction (both compounds are reduced at $E_{1/2} = -0.26$ V in this solvent), but other [Py_8TPyzPzM] derivatives with nonelectroactive metal ions such as M = $Mg^{II}(H_2O)$, Zn^{II}, or Cu^{II} compare better with respect to the absolute potential difference between half-wave potentials for the stepwise formation of the monoanion, dianion, trianion, and tetraanion.[1c] For example, the $\Delta E_{1/2}$ separation amounts to 0.40, 0.63, and 0.35 V for [Py_8TPyzPzPd] in pyridine as compared to quite similar average separations of 0.38, 0.63, and 0.30 V for the related Mg^{II}, Zn^{II}, and Cu^{II} complexes of Py_8TPyzPz (see Table 7). In addition, the $E_{1/2}$ values for each stepwise reduction of [Py_8TPyzPzM] become progressively less negative in pyridine as the metal ion is changed from Mg^{II} (−0.40 V) to Zn^{II} (−0.34 V), Cu^{II} (−0.30 V), and Pd^{II} (−0.26V), but this order in ease of reduction is not strictly followed in DMSO, where the Zn^{II} and Pd^{II} derivatives are both reduced at the same potential of −0.26 V (see Table 7).

[($PdCl_2$)$_4$$Py_8$TPyzPzPd]. As indicated in the Experimental Section, the pentapalladated [($PdCl_2$)$_4$$Py_8$TPyzPzPd] complex dissociates in pyridine, generating [Py_8TPyzPzPd] and $PdCl_2$, each of which was independently identified. Thus, as expected, the reduction of [($PdCl_2$)$_4$$Py_8$TPyzPzPd] in pyridine is characterized by four one-electron-transfer processes, which are associated with the monopalladated species (eqs 1–4) along with an irreversible two-electron reduction of each coordinated $PdCl_2$ group at a potential almost the same as that for the reduction of just $PdCl_2$ in the absence of the macrocycle. This is illustrated by the cyclic voltammograms in Figure 8. The peak potential for the reduction of the liberated $PdCl_2$ units coming from [($PdCl_2$)$_4$$Py_8$TPyzPzPd] ($E_p = -0.85$ V) in pyridine is almost identical with the peak potential for the reduction of $PdCl_2$ in the absence of the porphyrazine ($E_p = -0.83$ V) at a scan rate of 0.1 V s^{-1} (see Table 7). This result is as expected and is consistent with a loss of the four $PdCl_2$ groups in this solvent.

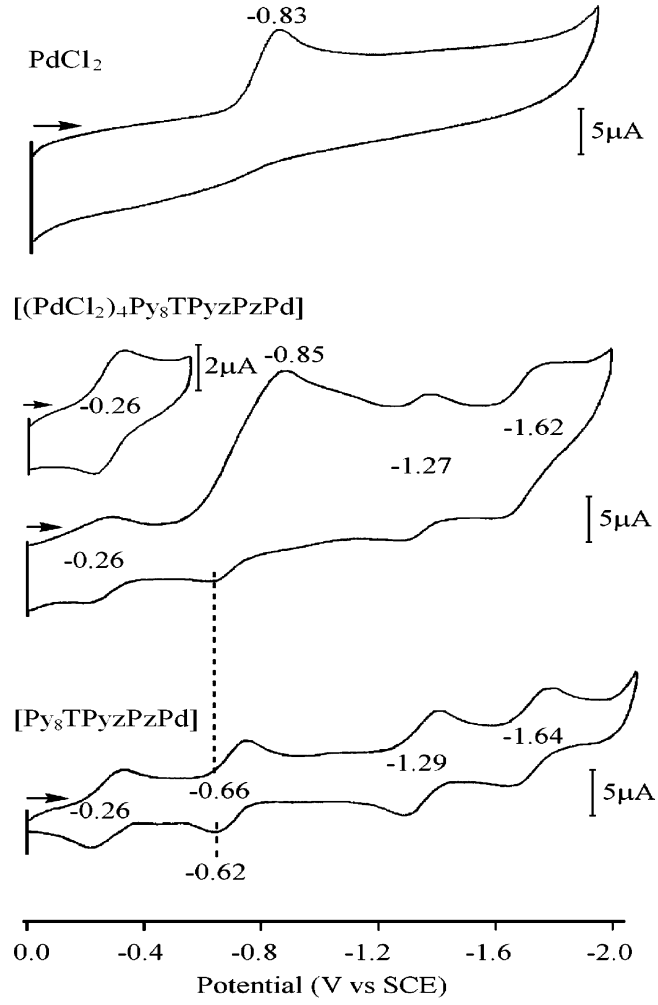

Figure 8. Cyclic voltammograms with added $E_{1/2}$ values (V vs SCE) showing the reduction of $PdCl_2$, [($PdCl_2$)$_4$$Py_8$TPyzPzPd], and [$Py_8$TPyzPzPd] (second scan) in pyridine containing 0.1 M TBAP. Scan rate = 0.1 V s^{-1}.

Cyclic voltammograms recorded on the first potential scan for the reductions of $PdCl_2$ and [($PdCl_2$)$_4$$Py_8$TPyzPzPd] and on the second scan potential after breaking the aggregates of [Py_8TPyzPzPd] are shown in Figures 9 (DMSO) and S3 in the Supporting Information (DMF). Unlike [Py_8TPyzPzPd], which is initially aggregated in the three nonaqueous solvents, no aggregation is observed for [($PdCl_2$)$_4$$Py_8$TPyzPzPd], probably due to steric hindrance from the four coordinated $PdCl_2$ groups.

As seen from Figure 9, Figure S3 in the Supporting Information, and Table 7, the first two reversible reductions of [($PdCl_2$)$_4$$Py_8$TPyzPzPd] are easier by 220−290 mV than the corresponding first two reductions of the monomeric monopalladated complex, a result clearly associated with exocyclic coordination of the $PdCl_2$ groups. Under these conditions, the first two electron additions can be described by eqs 5 and 6 and the last two by eqs 3 and 4.

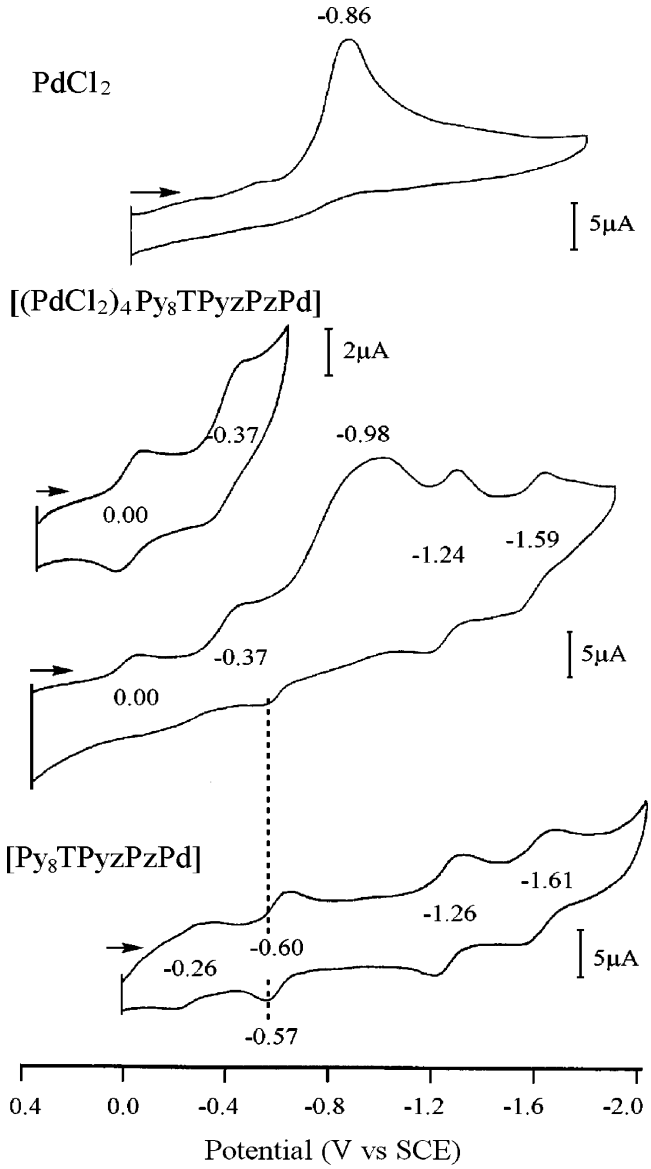

Figure 9. Cyclic voltammograms with added $E_{1/2}$ values (V vs SCE) showing the reduction of $PdCl_2$, $[(PdCl_2)_4Py_8TPyzPzPd]$, and $[Py_8TPyzPzPd]$ (second scan) in DMSO containing 0.1 M TBAP. Scan rate = 0.1 V s^{-1}.

$$[(PdCl_2)_4Py_8TPyzPzPd] \overset{e}{\rightleftharpoons} [(PdCl_2)_4Py_8TPyzPzPd]^- \quad (5)$$

$$[(PdCl_2)_4Py_8TPyzPzPd]^- \overset{e}{\rightleftharpoons} [(PdCl_2)_4Py_8TPyzPzPd]^{2-} \quad (6)$$

The two-electron reduction of each $PdCl_2$ group on $[(PdCl_2)_4Py_8TPyzPzPd]$ leads to Pd^0, which can form a film on the electrode surface, and this results in "distortion" of the current–voltage curve for the third and fourth macrocycle-centered reductions of the liberated monopalladated complex. Nonetheless, these reductions are reversible in DMF and DMSO and located at virtually the same half-wave potentials as those for reduction of $[Py_8TPyzPzPd]$, again consistent with a loss of the four $PdCl_2$ groups.

It should also be noted that a shift in E_p occurs for the irreversible reduction of the coordinated $PdCl_2$ groups of

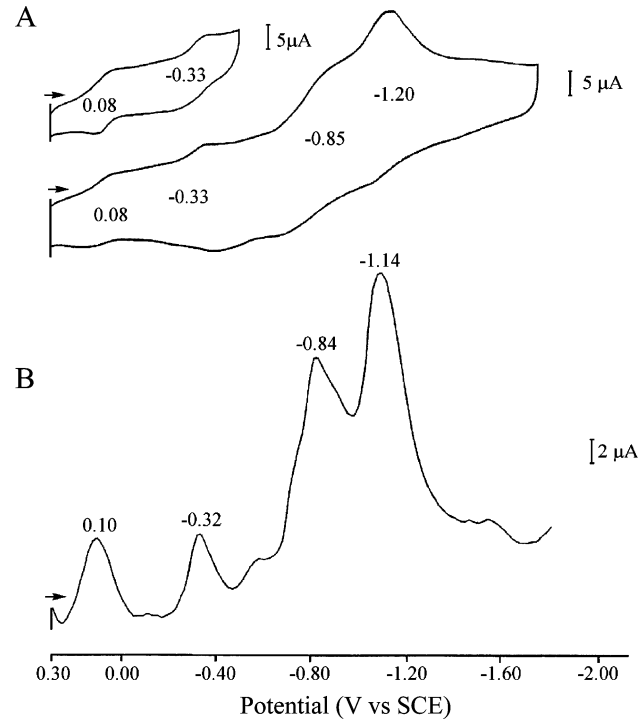

Figure 10. Cyclic voltammogram (A) and differential pulse voltammogram (B) (second scan) of $[(2\text{-Mepy})_8TPyzPzPd](I_8)$ in DMSO containing 0.1 M TBAP.

$[(PdCl_2)_4Py_8TPyzPzPd]$ as compared to the reduction of just $PdCl_2$. The coordinated $PdCl_2$ groups are reduced at $E_p = -0.98$ V in DMSO and -1.03 V in DMF for a scan rate of 0.1 V s^{-1} as compared to $E_p = -0.86$ V for the reduction of $PdCl_2$ in these two solvents in the absence of the macrocycle. Thus, the negative shift in $E_{1/2}$ for the reduction of coordinated $PdCl_2$ in these two solvents is consistent with the positive shift in $E_{1/2}$ for the first two reductions of the porphyrazine-centered reductions of the same compound, indicating a redistribution of negative charge density toward the $PdCl_2$ groups and away from the porphyrazine π-ring system. This is also seen in the enhancement of the macrocyclization-induced low-field shift of the ^1H NMR resonances of the pyridine rings. A shift of negative charge density from the porphyrazine π-ring system toward the $PdCl_2$ groups is also suggested by DFT results, showing that the peripherally coordinated $PdCl_2$ groups induce a significant stabilization of the LUMO and depletion of the electron density on the central Pd atom.

$[(2\text{-Mepy})_8TPyzPzPd](I)_8$. Cyclic voltammograms and differential pulse voltammograms illustrating the reduction of $[(2\text{-Mepy})_8TPyzPzPd](I)_8$ in DMSO containing 0.1 M TBAP are presented in Figure 10, where the current–voltage curves were recorded on the second potential sweep from +0.30 to −1.80 V. Under these experimental conditions, the compound undergoes two well-defined one-electron reductions at $E_{1/2} = +0.08$ and -0.33 V followed by multiple electron transfers at more negative potentials (Figure 10A). The first two reductions of $[(2\text{-Mepy})_8TPyzPzPd]^{8+}$ are assigned as processes occurring at the conjugated π-ring system of the macrocycle and occur as shown in eqs 7 and 8.

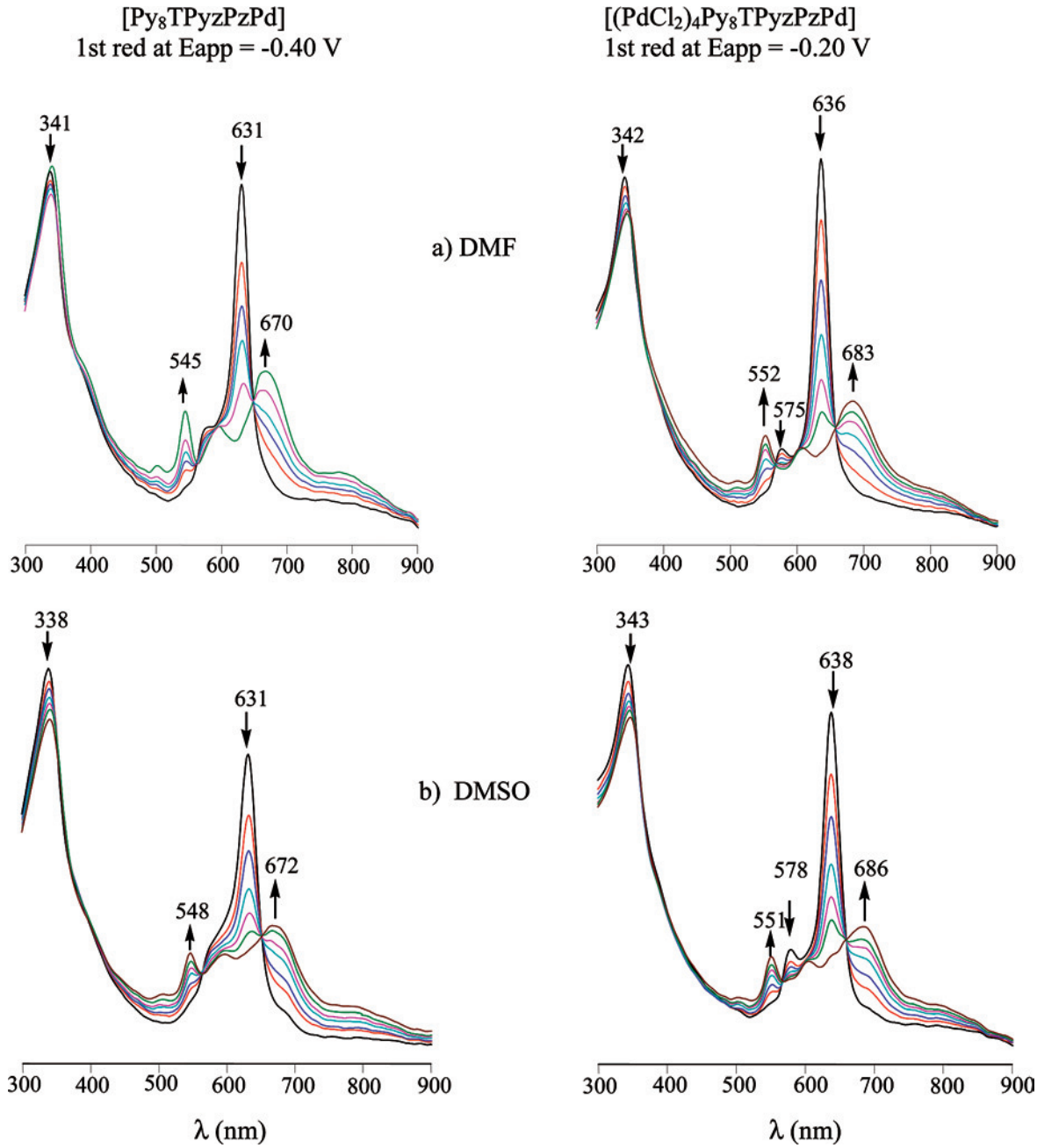

Figure 11. UV–visible spectral changes during first reduction of $[Py_8TPyzPzPd]$ and $[(PdCl_2)_4Py_8TPyzPzPd]$ in (a) DMF and (b) DMSO containing 0.2 M TBAP. The spectra of $[Py_8TPyzPzPd]$ were recorded after an initial reduction at –1.40 V followed by reoxidation at 0.0 V to generate the monomeric species in solution.

$$[(2\text{-Mepy})_8TPyzPzPd]^{8+} \overset{e}{\rightleftharpoons} [(2\text{-Mepy})_8TPyzPzPd]^{7+} \quad (7)$$

$$[(2\text{-Mepy})_8TPyzPzPd]^{7+} \overset{e}{\rightleftharpoons} [(2\text{-Mepy})_8TPyzPzPd]^{6+} \quad (8)$$

Voltammograms were also recorded on an initial scan from +0.30 to −1.80 V, but under these experimental conditions, the currents for conversion of $[(2\text{-Mepy})_8TPyzPzPd]^{8+}$ to $[(2\text{-Mepy})_8TPyzPzPd]^{7+}$ (eq 7) are enhanced as a result of the catalytic process involving the singly reduced porphyrazine and some form of iodine in solution, which leads to a distorted current–voltage curve as shown in Figure S4 of the Supporting Information.

Table 8. UV–Visible Spectral Data [λ, nm (log ϵ)] of the Singly Reduced Compounds in Different Solvents Containing 0.2 M TBAP

solvent	compound[a]	Soret region	Q-band region		
py	$[LPd]^-$	340(5.05)	550 (4.57)	600 (4.45)	672 (4.79)
	$[(PdCl_2)_4LPd]^-$	340(5.22)	550 (4.72)	600 (4.68)	672 (4.86)
	$[L'Pd]^{7+}$	338(5.09)	565 (4.42)		690 (4.39)
DMSO	$[LPd]^-$	342(5.11)	548 (4.53)	591 (4.50)	672 (4.64)
	$[(PdCl_2)_4LPd]^-$	347(5.18)	551 (4.52)	605 (4.48)	686 (4.68)
	$[L'Pd]^{7+}$	340(5.14)	555 (4.01)	607 (4.24)	691 (4.17)
DMF	$[LPd]^-$	341(5.07)	545(4.24)	593 (4.33)	70 (4.68)
	$[(PdCl_2)_4LPd]^-$	345(5.17)	552 (4.64)	605 (4.59)	683 (4.78)
	$[L'Pd]^{7+}$	340(5.21)	552 (4.42)		685 (4.43)

[a] L = $Py_8TPyzPz$; L′ = $(2\text{-Mepy})_8TPyzPz$.

Further reductions after generation of $[(2\text{-Mepy})_8TPyzPzPd]^{6+}$ occur at potentials between −0.84 and −1.14

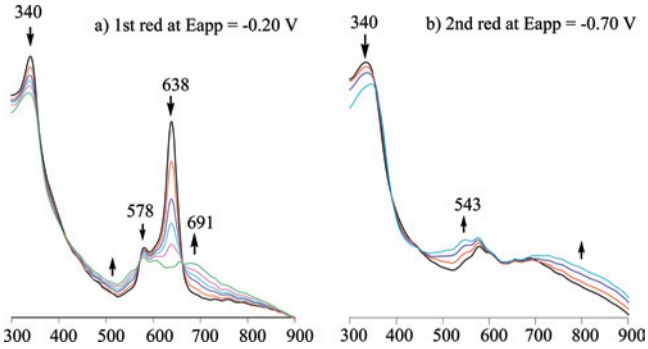

Figure 12. UV–visible spectral changes during (a) the first and (b) the second reductions of $[(2\text{-Mepy})_8\text{TPyzPzPd}](I)_8$ in DMSO containing 0.2 M TBAP. The spectra were recorded after initially applying a potential of +0.30 V in order to convert all of the compound to its fully unreduced form.

V, and these are assigned as reactions involving the NCH_3^+ substituents. The eight positively charged NCH_3^+ groups on $[(2\text{-Mepy})_8\text{TPyzPzM}]^{8+}$ should each be reduced by one electron,[27] and this seems to be the case in Figure 10B, where the ratio of integrated current for all processes between −0.45 and −1.70 V is approximately 10 times the integrated current of the first reduction, consistent with the addition of 12 electrons overall, 8 on the NCH_3^+ groups, and 4 on the conjugated macrocycle of $[(2\text{-Mepy})_8\text{TPyzPzM}]^{8+}$.

In the present paper, we have concentrated only on the first two ring-centered reductions of $[(2\text{-Mepy})_8\text{TPyzPzPd}]^{8+}$ (eqs 7 and 8), both of which are extremely facile in the three utilized solvents (py, DMSO, and DMF) as compared to $[\text{Py}_8\text{TPyzPzPd}]$ (eqs 1 and 2). The first two reductions of $[(2\text{-Mepy})_8\text{TPyzPzPd}]^{8+}$ are also slightly more positive than $E_{1/2}$ for reduction of $[(\text{PdCl}_2)_4\text{Py}_8\text{TPyzPzPd}]$ or other previously investigated $[(2\text{-Mepy})_8\text{TPyzPzM}]^{8+}$ compounds under the same solution conditions.[1e] For example, the half-wave potentials in DMSO for reduction of $[(2\text{-Mepy})_8\text{TPyzPzM}]^{8+}$ with different metal ions follow the order Pd^{II} (0.08 V) > Cu^{II} (−0.04 V) > Zn^{II} (−0.10 V) > Mg^{II} (−0.19 V), and the same order is seen in the second reduction, where $E_{1/2}$ = −0.33 V for generation of $[(2\text{-Mepy})_8\text{TPyzPzPd}]^{6+}$ as compared to −0.38 V (Cu^{II}), −0.44 (Zn^{II}), and −0.47 V (Mg^{II}). These values are listed in Table 7.[1e]

In summary, quaternization of the external pyridine N atoms and formation of the octacationic complex $[(2\text{-Mepy})_8\text{TPyzPzPd}]^{8+}$ enhance the overall electron-withdrawing properties of the macrocycle similar to what is obtained upon exocyclic coordination of $PdCl_2$ by $[\text{Py}_8\text{TPyzPzPd}]$. This is perfectly in line with findings for a parallel series of previously investigated $[\text{Py}_8\text{TPyzPzM}]$ complexes and with related octacations[1e] with different M^{II} central metal ions.

Spectroelectrochemistry. Thin-layer UV–visible spectra were obtained for singly and doubly reduced $[\text{Py}_8\text{TPyzPzPd}]$, $[(\text{PdCl}_2)_4\text{Py}_8\text{TPyzPzPd}]$, and $[(2\text{-Mepy})_8\text{TPyzPzPd}]^{8+}$ in the three solvents (pyridine, DMSO, and DMF). Examples of the UV–visible spectral changes for $[\text{Py}_8\text{TPyzPzPd}]$ and $[(\text{PdCl}_2)_4\text{Py}_8\text{TPyzPzPd}]$ during the first one-electron reduction in DMF and DMSO are illustrated in Figure 11, while spectral data for the reduction of $[\text{Py}_8\text{TPyzPzPd}]$ and $[(\text{PdCl}_2)_4\text{Py}_8\text{TPyzPzPd}]$ in pyridine are shown in Figure S5 in the Supporting Information.

The basic common feature of the monoanion in all three solvents is a loss of the Q band and the appearance of new absorptions in the region 500–900 nm (see Table 8). These spectral features of the porphyrazine monoanion generally parallel what has been reported for other electroreduced $[\text{Py}_8\text{TPyzPzM}]$ species,[1c] with the main difference being a sharp absorption at ca. 340–345 nm, of intensity comparable to that of the Q band. The first two reductions of $[\text{Py}_8\text{TPyzPzPd}]$ and $[(\text{PdCl}_2)_4\text{Py}_8\text{TPyzPzPd}]$ are both reversible, and the UV–visible spectrum of the initial compound in its monomeric form could be obtained upon reoxidation at an appropriate applied potential.

The reduction of $[(2\text{-Mepy})_8\text{TPyzPzPd}]^{8+}$ to its $[(2\text{-Mepy})_8\text{TPyzPzPd}]^{7+}$ form in the thin-layer cell results in similar spectral changes as in the case of $[\text{Py}_8\text{TPyzPzPd}]$ and $[(\text{PdCl}_2)_4\text{Py}_8\text{TPyzPzPd}]$, but less well-defined spectral features are seen after the addition of a second electron, as shown in Figure 12, parts a and b. The spectrum of the unreduced cation $[(2\text{-Mepy})_8\text{TPyzPzPd}]^{8+}$, like for $[\text{Py}_8\text{TPyzPzPd}]$ and $[(\text{PdCl}_2)_4\text{Py}_8\text{TPyzPzPd}]$, has three analogous bands in this case located at 340, 578, and 638 nm, while the singly reduced compound shows the complete disappearance of the Q band and a new absorption at 691 nm in addition to other reduced intensity bands between 500 and 900 nm.

Conclusions

The present study describes the synthesis and physicochemical characterization of novel penta- and monopalladated species having the formula $[(\text{PdCl}_2)_4\text{Py}_8\text{TPyzPzPd}]$, $[\text{Py}_8\text{TPyzPzPd}]$, and $[(2\text{-Mepy})_8\text{TPyzPzPd}](I)_8$. The complexes are easily synthesized under mild conditions and obtained in good yield as air-stable materials.

The structural features of the $[(\text{PdCl}_2)_4\text{Py}_8\text{TPyzPzPd}]$ complex were elucidated through one- and two-dimensional ^{1}H NMR spectra in solution, DFT calculations, X-ray data, and solution ^{1}H NMR spectra of the $[(\text{CN})_2\text{Py}_2\text{PyzPdCl}_2]$ precursor, whereas structural information on the monopalladated complex $[\text{Py}_8\text{TPyzPzPd}]$ was obtained from DFT calculations. In particular, it was found that, in the pentapalladated complex, the peripheral $PdCl_2$ units adopt a py−py coordination mode, and the square-planar N_2PdCl_2 moieties are directed nearly perpendicular to the plane of the pyrazinoporphyrazine ring. NMR and DFT results consistently indicated that, of the four structural isomers, which are likely to be generated during the synthetic procedure of the pentapalladated complex, the 4:0 isomer (C_{4v} symmetry) is the prevalent one in solution. A detailed electrochemical and spectroelectrochemical study provided information on the capability of the macrocycles to undergo up to four reversible or quasi-reversible reductions at the conjugated π-ring system

(27) (a) Kadish, K. M.; Sazou, D.; Liu, M.; Guilard, R. *Inorg. Chem.* **1988**, *27*, 686. (b) Kadish, K. M.; Araullo, C.; Guilard, R. *Inorg. Chem.* **1989**, *28*, 2528. (c) Araullo, C.; Kadish, K. M. *Inorg. Chem.* **1990**, *29*, 2749. (d) Van Caemelbecke, E.; Kunter, W.; Kadish, K. M. *Inorg. Chem.* **1993**, *32*, 438. (e) Van Caemelbecke, E.; Hambright, D.; Garcia, R.; Kadish, K. M. *Inorg. Chem.* **2005**, *44*, 3789.

plus additional reactions at the four coordinated $PdCl_2$ units in the $[(PdCl_2)_4Py_8TPyzPzPd]$ complex. For the most stable structural components present in $[(PdCl_2)_4Py_8TPyzPzPd]$ and $[Py_8TPyzPzPd]$ in solution, a detailed theoretical analysis of the ground-state electronic structure was performed, which allowed for a rationalization of the tendency of these complexes to undergo more facile stepwise reductions and more difficult oxidations as compared to mononuclear phthalocyanine complexes, including [PcPd]. Electronic structure calculations also provided an explanation for the fine details of the electrochemical behavior of the pentapalladated complex in terms of the electronic interactions between the macrocyclic ring and the peripheral $PdCl_2$ fragments.

Our studies of the synthesized palladium(II) species were further extended to an investigation of their behavior as photosensitizers for the production of singlet oxygen, $^1O_2$, and the results of these studies will be reported in a forthcoming paper.[3]

Acknowledgment. Support by the University of "La Sapienza", MIUR (C.E., Cofin 2003038084), and the Robert A. Welch Foundation (K.M.K., Grant E-680) is gratefully acknowledged. The authors are highly indebted to Prof. F. Monacelli and Dr. C. Bergami for their contributions and suggestions during the development of this work and to Dr. G. Caruso for assistance and discussion of the MALDI-TOF experiments.

Supporting Information Available: X-ray crystallographic data in CIF format, Figures S1 and S2, details of the X-ray data collection and structure analysis, Tables S1 and S2 containing experimental data and relevant conformational parameters of $[(CN)_2Py_2PyzPdCl_2]$, cyclic voltammograms of $PdCl_2$, $[(PdCl_2)_4Py_8TPyzPzPd]$, and $[Py_8TPyzPzPd]$ in DMF (Figure S3), cyclic voltammogram and differential pulse voltammogram (first scan) of $[(2\text{-}Mepy)_8TPyzPzPd](I)_8$ in DMSO (Figure S4), and UV–visible spectral changes of the first reduction of (a) $[Py_8TPyzPzPd]$ and (b) $[(PdCl_2)_4Py_8TPyzPzPd]$ in pyridine (Figure S5). This material is available free of charge via the Internet at http://pubs.acs.org.

IC702430J